UCLA-ENG-8838
December 1988

EXPERIMENTS WITH METALLIC AND CERAMIC POROUS MEDIA

REPORT

December 30, 1988

by

T. H. K. Frederking, Principal Investigator
P. Abbassi
P. K. Khandhar
Jack Luna

PREPARED FOR THE
NATIONAL AERONAUTICS AND SPACE ADMINISTRATION
AMES RESEARCH CENTER
MOFFETT FIELD, CA 94035

GRANT NAG 2-516

Department of Chemical Engineering
School of Engineering and Applied Science
University of California, Los Angeles, CA 90024

UCLA-ENG-8838
December 1988

EXPERIMENTS WITH METALLIC AND CERAMIC POROUS MEDIA

REPORT

December 30, 1988

by

T. H. K. Frederking, Principal Investigator
P. Abbassi
P. K. Khandhar
Jack Luna

PREPARED FOR THE
NATIONAL AERONAUTICS AND SPACE ADMINISTRATION
AMES RESEARCH CENTER
MOFFETT FIELD, CA 94035

GRANT NAG 2-516

Department of Chemical Engineering
School of Engineering and Applied Science
University of California, Los Angeles, CA 90024

1. ABSTRACT

Work in the area of mechano-caloric phenomena has been initiated during 1988 with startup in the Summer 1988 period. The ideal system utilizing He II "super-phenomena" is modeled readily, within the frame of thermodynamics energetics, using the concept of an ideal superleak. The real system however uses porous media of non-ideal pore-grain ingredients. The early phase of experimental and related modeling studies is outlined for the time period from Summer 1988 to the end of 1988.

TABLE OF CONTENTS

2. INTRODUCTION

The project has been started up with the goal of obtaining realistic performance values of a mechano-caloric component. The mechano-caloric effect has been documented in the early literature on the subject[1]. The effect is one particular phenomenon out of several peculiar properties of "superfluids". The spectacular property of "superfluidity" has been reported in 1938 by Kapitza and Allen and Misener. The latter authors used a bundle of fine stainless steel wires, packing it into a thick walled, low-conductivity alloy tube ("German silver"), and drawing the system down to a small diameter. The result had been a set of channels between the wires with not more than one micro-meter in diameter. Similarly, Kapitza experimented with annuli arranged to have a distance, between walls, on the order of magnitude 1 micro-meter or less. The velocity of flow of liquid He II (i.e. Helium-4 below its lambda point), turned out to be nearly *independent* of an externally applied pressure head. This unusual property has been referred to as "superfluidity". If flow rates are unaffected by the driving force, the flow resistance commonly observed does not exist. Hence the term superfluid liquid Helium appears to be justified.

The next most important "new effect" found with liquid He II has been the thermomechanical effect: a difference temperature (ΔT), applied externally by suitable means, causes a pressure difference (ΔP). The first observations have been reported by Allen and Jones[2]. The thermomechanical pressure difference in these early experiments has been converted to kinetic energy associated with a "fountain" of liquid He II. Hence the term fountain effect has become popular as well. The presently accepted two-fluid model macroscopics postulates a simple description involving two separate fluid components (normal and superfluid). The additional postulate of "zero chemical potential difference" ($d\mu = 0$) for this system leads to the famous H. London equation (e.g. Wilks, 1967)[3]. The result of thermostatic conditions is

$$(\partial P/\partial T)_\mu = \rho S \tag{2.1}$$

(ρ liquid density, S entropy per unit/mass of liquid).

As noted by Wilks (op. cit. above), there is a corollary to the thermomechanical experiments: an application of an externally applied pressure difference (head) may lead to heating or to cooling. Equation (2.1) is rewritten in the form

$$(\partial T/\partial P)_\mu = 1/(\rho S) \tag{2.2}$$

When the pressure increment is $dP > 0$, the incremental temperature change has to be $dT > 0$, i.e. heating is observed. When the pressure drops however, ($dP < 0$), there is a decrease $dT < 0$. This implies mechano-caloric cooling. This effect was observed first by Daunt and Mendelssohn[4].

The two-fluid interpretation is as follows: only superfluid, devoid of viscosity, will flow through the narrow fluid passages cited above. The consequence is an enrichment of normal fluid on the other side of the passages. An increase in normal fluid "concentration" means an enhanced temperature. If the sign changes such that superfluid flows into the fluid space considered, a drop in T occurs. Thus, cooling may be accomplished in a refrigerator, e.g. the He II "vortex fridge" (Staas–Severijns,1969)[5].

3. 1988 PROGRESS AND DISCUSSION

The preceding section points out the potential use of the He II "supereffects" in unique refrigeration devices called He II vortex refrigerators. Their components are the pump (possibly a thermomechanical effect device), and a mechano-caloric component. During the work done up to this time, it became clear to us that a careful plug selection is possible only when irreversibilities along with most favorable thermodynamic parameters are known. The following topics are considered: phenomenology of porous media, metal porous plugs at zero net mass flow (ZNMF), and ceramic plugs at ZNMF.

Phenomenology of porous media. Figure 1a is a schematic diagram of the ideal and real pressure difference (static case) of a He II thermomechanical pump (fountain effect pump, FEP). Figure 1b schematically presents a similar mechano-caloric component (MCC) diagram. Figure 1a indicates that the ideal superleak case (ISL) is an upper bound for an extended temperature difference. Irreversibilities at large ΔT cause a saturation in the static ΔP.

Figure 1b indicates that the ISL temperature difference predicted is an upper bound to the real ΔT when irreversibilities cause a less efficient change of state than the ISL case. Figure 2 is a plot of the pressure increase of the ideal pump (ISL) for various initial bath temperatures. Figure 3 is a plot of the ideal lowering of the temperature in a mechano-caloric component (ISL case). The consequence of the calculations and of early data is a need to get experimental evaluations of particular plug materials for each case. Furthermore, it is necessary to obtain a unique measure of the liquid throughput capability in a real plug. The quantity chosen is the Darcy permeability of a porous medium. The so-called Zero Net Mass Flow (ZNMF) technique has been used in order to characterize the plugs employed in the research. Details of these studies are outlined in the Appendix sections A and B.

Metal porous plugs at ZNMF. The present metal systems are in a permeability range below the more thoroughly documented plug range of vapor-liquid phase separators. The latter have been described in earlier work, e.g. the Ph.D. thesis of Dr. Sidney Yuan (UCLA, 1985). Figure 4 is a characteristic length diagram from the M.S. thesis of P. Khandhar. The abstract of the thesis is attached as Appendix D. The present work suggests that metal plug manufacturers have improved their fabrication capabilities. They produce well-defined plugs in the Darcy permeability (order of magnitude) range of $\kappa \sim 10^{-10}$ cm^2, while several years ago 10^{-8}–10^{-9} cm^2 was available only.

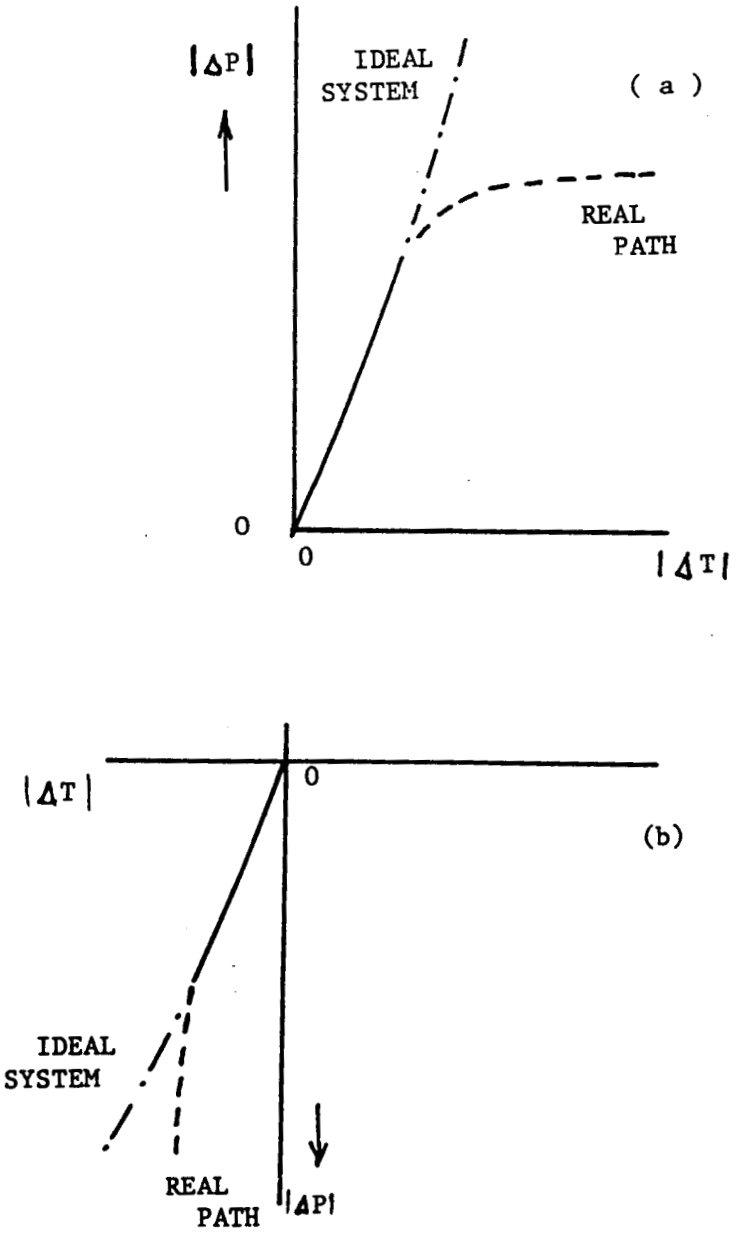

Fig. 1. Schematic diagram of (absolute) temperature difference (ΔT) and pressure difference (ΔP) behavior.
a. fountain effect pump (FEP)
b. mechano-caloric component (MCC)

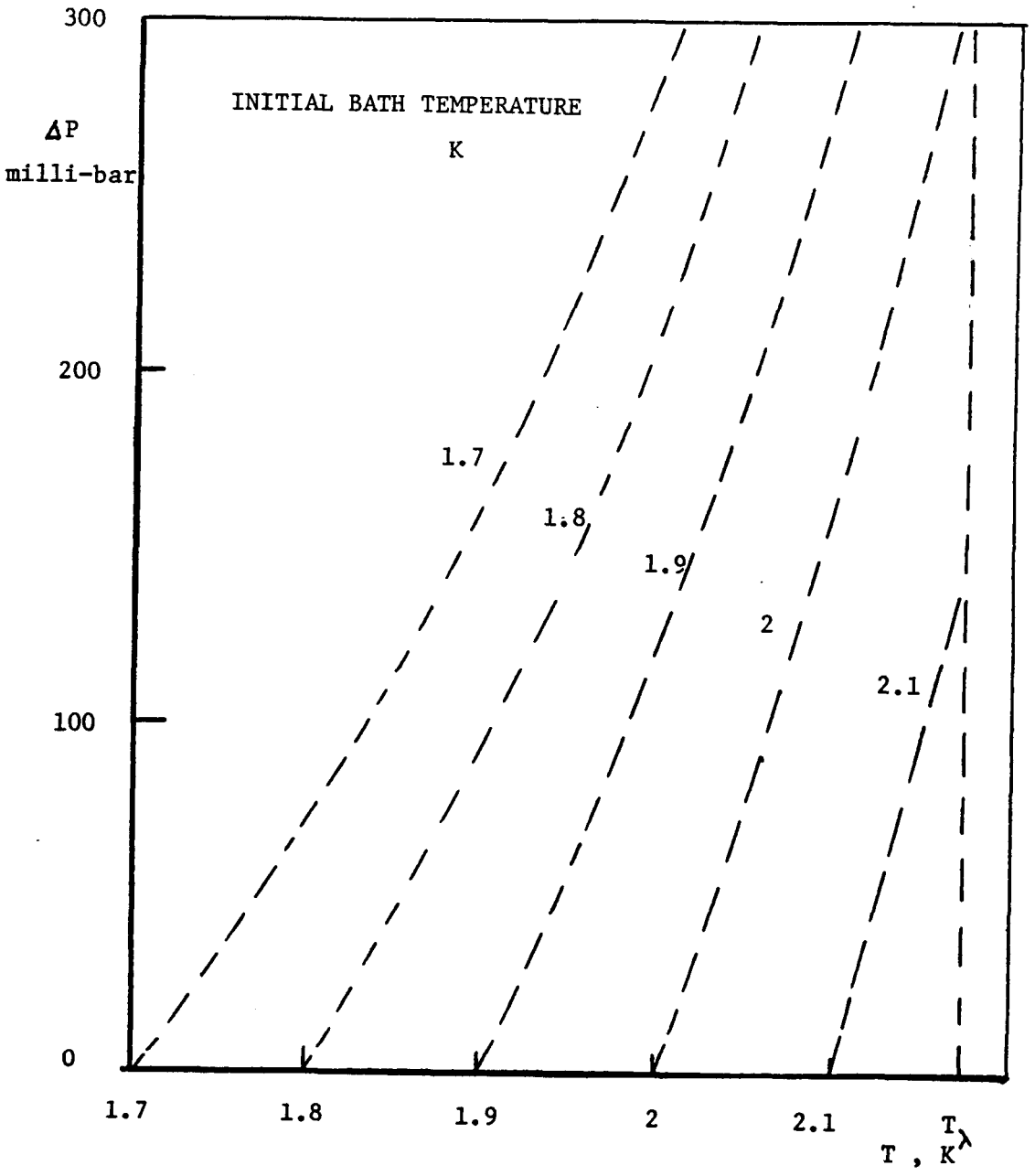

Fig. 2. Pressure increase of the ideal FEP based on the ideal superleak (ISL) concept.

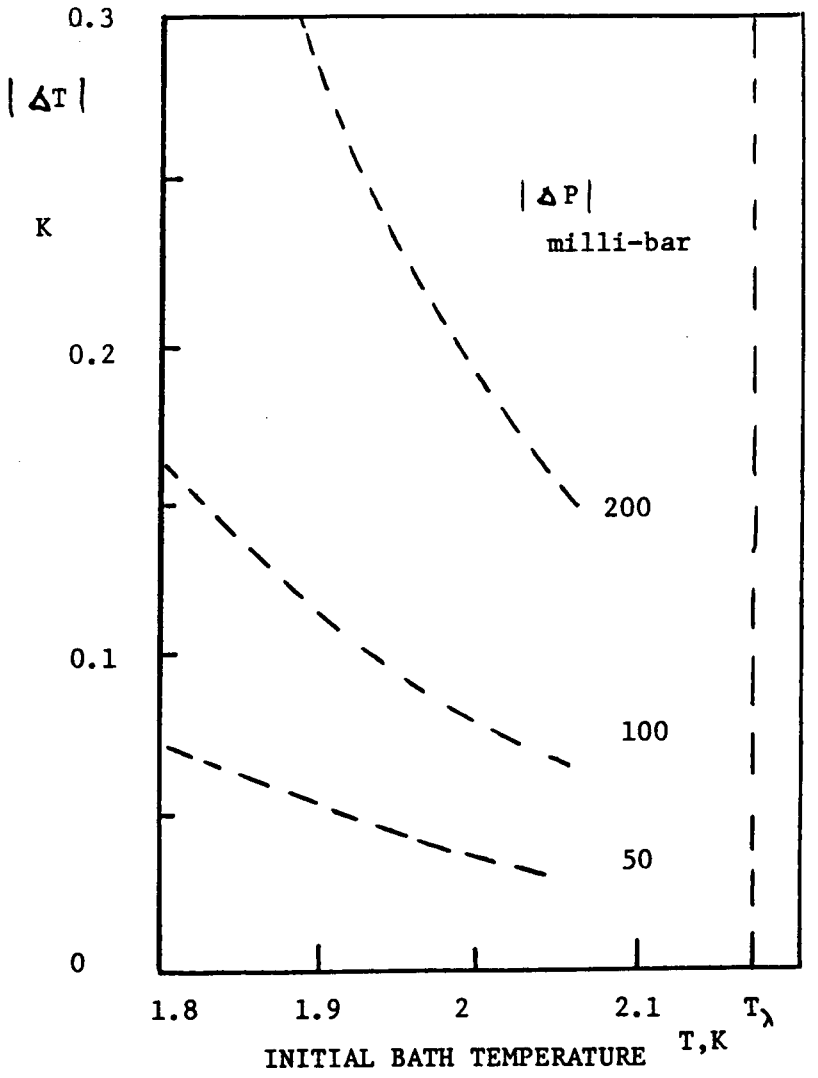

Fig. 3. Lowering of the temperature in an ISL system

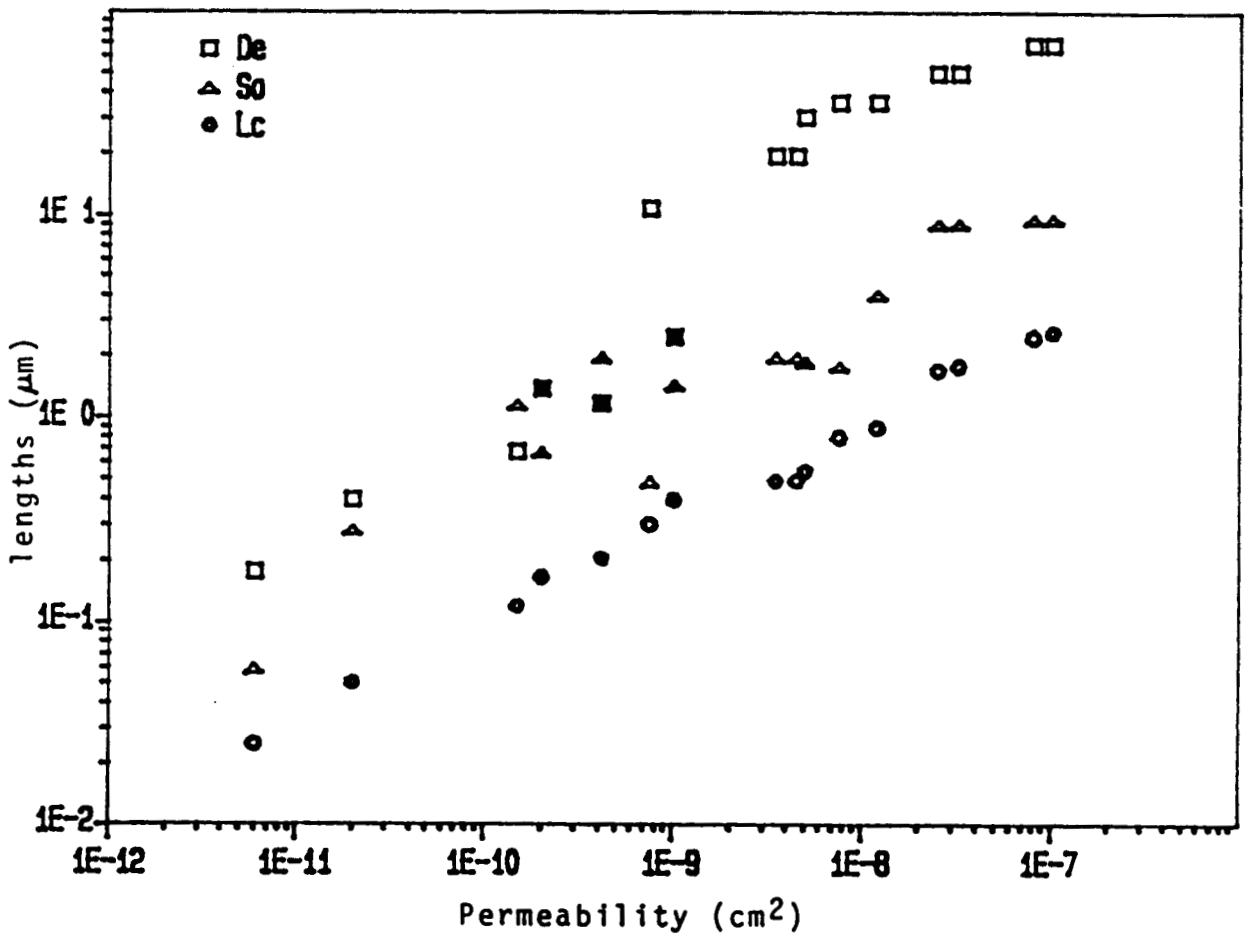

Fig. 4. Characteristic length diagram of porous media (from M.S. thesis of P. Khandhar, 1989).
L_c characteristic length
S_o filtration rating, D_e equivalent particle diameter of an ideal packed bed

Figure 4 contains packed bed ceramic plugs of Singsaas (Ref. 6). These plugs have been considered less desirable for space conditions than rigid plugs whose particles are set. In addition some mechanical rigidity without excessive exposure to forces appears to be useful. While the metal plugs are documented in the Appendix sections A and B, the ceramic experiments have been in a rather early stage.

Ceramic plug at ZNMF. We have used two ceramic plug systems. One has been cooled down only to the liquid nitrogen range. The other one has been subjected to liquid Helium conditions.

Both plugs are units manufactured by Coors Ceramic Corp., Golden, Colorado. The ceramic components designed for filtration purposes have the shape of a cylindrical cup, open at one end. The geometry does not have a perfect cylindrical shape because of firing constraints after initial shaping. Two cups are joined together as shown schematically in Figure 5.

A phenolic ring (PR) has a dual purpose. First, for low heat leakage it has a small non-porous area (compared to the total cup area available for porous media flow); second, the various instrument wires are routed through the ring. Instrumentations include an internal heater unit (IHU), a pressure transducer (PD) (Siemens KPY type), and a carbon thermometer (C-TH).

Pressure transducer characteristics have been determined*. An example is Figure 6. Various results obtained appear to be consistent with early manufacturer data[7].

Results obtained with the second sup set are presented in Figure 7 as pressure transducer response as a function of the heat input during the ZNMF runs. These data are for rather high heat inputs (compared to the critical rates, estimated for these rather fine plugs). When the plug unit had been warmed up, after the He II runs, it turned out that there were cracks visible after a thorough room temperature inspection. Areas detected have been covered with epoxy. After a

*Dr. A. Elsner has dynamically contributed to the early pressure transducer studies, and his effort is acknowledged with appreciation.

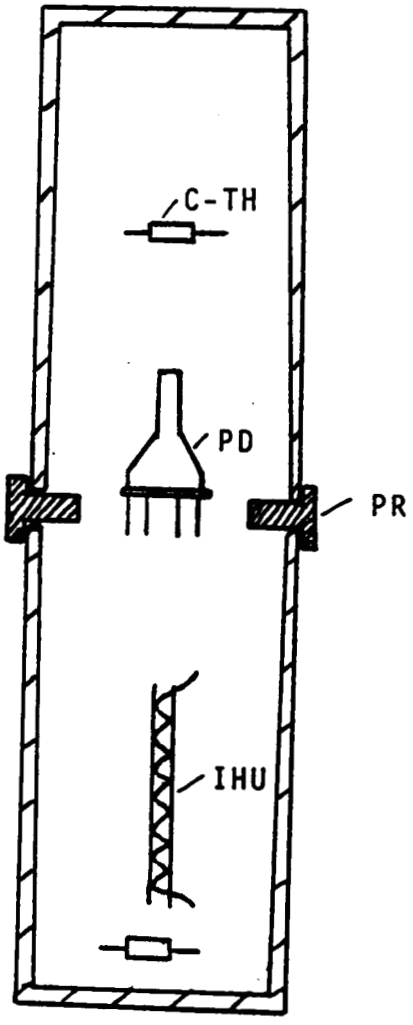

Fig. 5. Ceramic porous filter cup geometry, schematically. PR phenolic ring, IHU internal heater unit, C-TH carbon thermometer, PD pressure transducer.

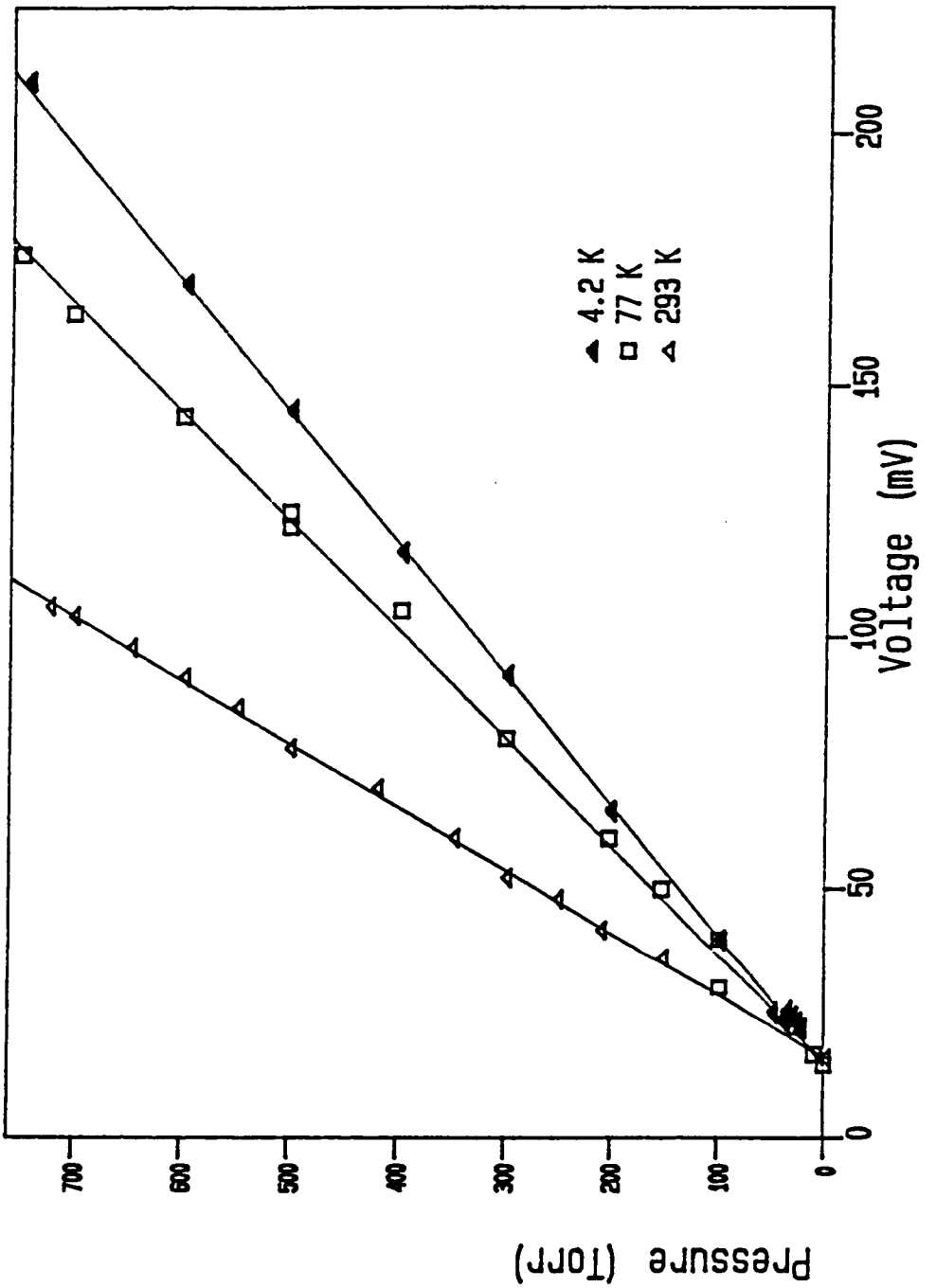
4.2 K
77 K
293 K
Voltage (mV)
Pressure (Torr)
0
50
100
150
200
0
100
200
300
400
500
600
700

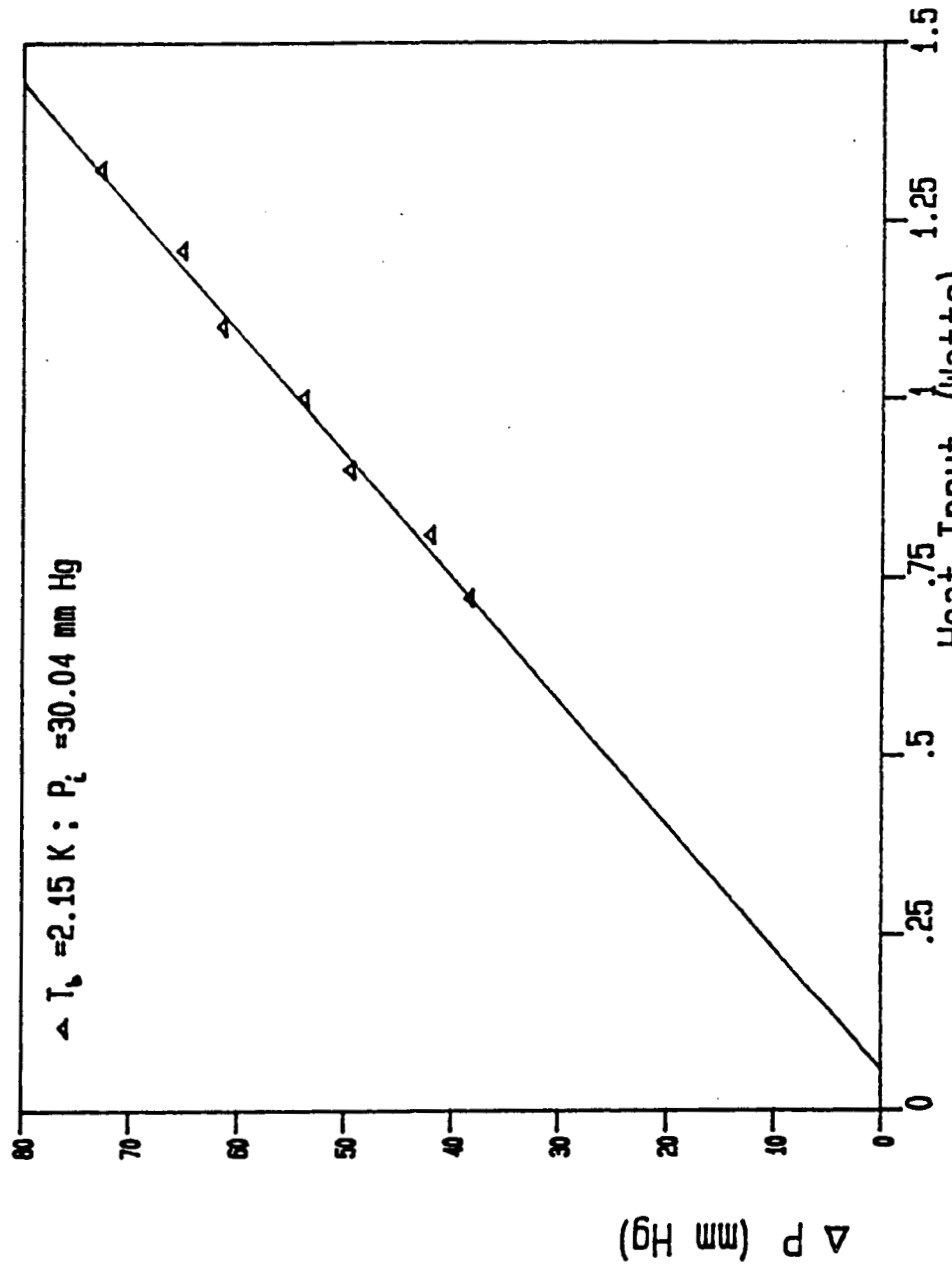

Fig. 7. Pressure transducer results during ZNMF runs at high heat inputs.

second set of runs, the same type of cracks had been formed again. The room temperature inspection showed additional local domains where ceramic material had fractured on the cup surface. Chips, found below the plug/cup system, have been an indication of the brittle nature of the ceramics and related lack of mechanical reliability. It is noted that this type of potential fracture danger is inherent in the recently discovered metal oxide superconductors with high transition temperature (HTSC). The assessment of HTSC has been the topic of a recent seminar on heat transfer related to stability of superconducting magnets. This work is outlined in Appendix C.

Plug data have been collected for various heat inputs $\dot{Q}$ into the porous plug chamber at different bath temperature. Examples of data are presented in Figs. 8 and 9;(A total plug cross section). $\dot{Q}/A$ versus temperature difference is presented in Fig. 8. The data indicate a linear region in the ZNMF mode at low $\dot{Q}$. Figure 9 represents the data in the ΔT range from 0 to 100 mK. The data appear to be mostly in the non-linear range.

Acknowledgments. The contributions of Dr. A. Elsner and of our collaborators David Y. Ono and F. Afifi are acknowledged with thanks.

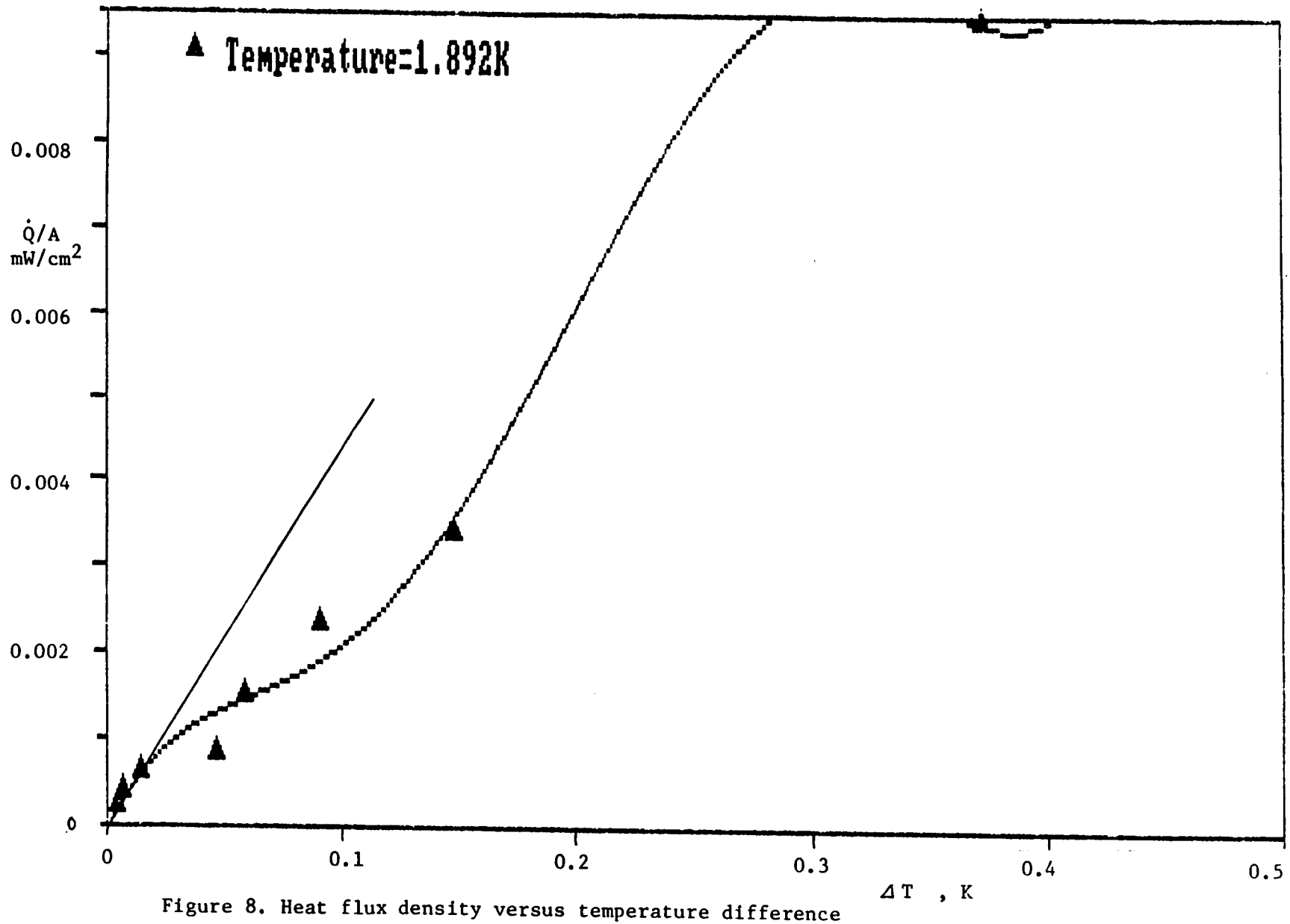

Figure 8. Heat flux density versus temperature difference

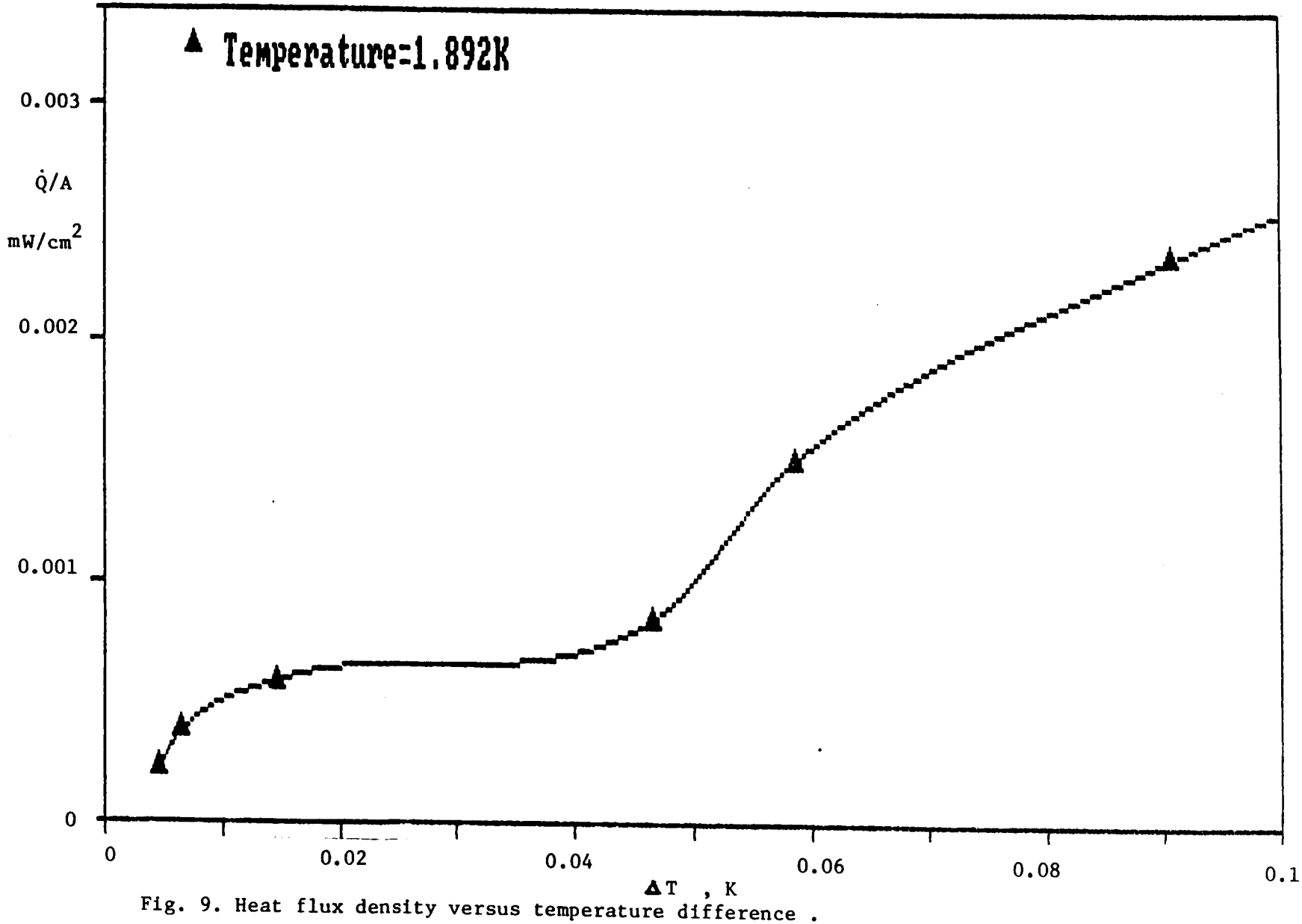

Fig. 9. Heat flux density versus temperature difference .

4. REFERENCES

1. K. R. Atkins, Liquid Helium, Cambridge University Press, 1959.
2. J. F. Allen and H. Jones, Nature, 141, 243, 1938.
3. J. Wilks, The Properties of Liquid and Solid Helium, Oxford University Press, 1967.
4. J. G. Daunt and K. Mendelssohn, Nature, 143, 719, 1939.
5. F. A. Staas and A. P. Severijns, Cryogenics, 9, 422, 1969.
6. A. L. Singsaas, Ph.D. Thesis, Santa Barbara, 1984.
7. F. Breimesser, L. Intichar, M. Poppinger and C. Schnapper, J. de Phys. p. C1-671, 1983.

APPENDIX A

ONSET OF VAPORIZATION ASSOCIATED WITH COUNTERFLOW IN POROUS MEDIA

T. H. K. Frederking, P. K. Khandhar, P. Abbassi

University of California, Los Angeles, CA 90024

Porous sintered metal plugs have been subjected to counterflow. A step input in power is applied to a heater inside a He I chamber which is connected via the plug to an external He II bath. Phenomena of phase transitions are analyzed on the basis of thermograms obtained (chamber liquid temperature vs. time data for relatively large diameter ducts): there is He II superheating across the first order transition phase boundary, of the vapor pressure curve. For high heat inputs, extended vapor domains are produced in the chamber for temperatures above the homogeneous nucleation limit.

INTRODUCTION

He II fluid management and thermal control involving porous media devices have been receiving increased attention. Furthermore, the use of narrow coolant channels in magnets produces a special type of "porous" structure. The operation of these systems in metastable liquid states, beyond the equilibrium state phase boundaries has been the topic of several recent studies [1-6]. The present studies have the purpose of extending the geometries covered to include porous media. The following phenomena are encountered:

Various types of superheating of He II and He I;
Phase transition involving metastable liquid below the saturated liquid lambda point pressure;
Phase transitions leading to high temperature excursions into the vapor domain.

PHASE TRANSITION PHENOMENA INVOLVING FLUIDS (He^4)

The studies cited in references 1-6 have clarified details of phase changes during heat flow in duct systems. The findings are briefly outlined, emphasizing pressures (P) below $P_{\lambda,sat}$, where $P_{\lambda,sat}$ is the lambda point pressure of saturated He II at liquid He II-He I-vapor equilibrium. For $P > P_{\lambda,sat}$, there has been no superheating of He II to metastable He II states beyond the lambda line during heating. Instead He I domains are formed when the liquid is heated to T > T lambda (P). At $P < P_{\lambda,sat}$, the following phenomena have been observed [1-5]: During a finite duration of time (t), He II may be heated up, in a local "hot" domain across the first order phase transition taking place at the vapor pressure curve. This involves the latent heat of vaporization on the order of 20 J/(g K).

According to theoretical and experimental results, the metastable He II cannot be superheated (in a He II state) beyond the lambda line extension from $P_{\lambda,sat}$ to low P. This line is very steep in the P(T) phase diagram, and T lambda is near 2.172 K.

Metastable He I may be formed at "high T" states, beyond the extended lambda line, in heated domains. From this metastable He I, vapor bubbles of nucleate boiling may be formed ("triple-phase nucleate boiling", ref. 7). The nucleate boiling mode is quite efficient in keeping the temperature at a heater at low T, close to the Kapitza-resistance-dominated solid temperature.

Metastable He I, upon heating at a high heat flux density q, may be converted into "hot" vapor domains at which point the homogeneous nucleation line is traversed during the temperature excursion T(t). The process leads to low film boiling rates ("triple-phase film boiling") of heat removal, or high local temperatures at the heater.

*) Presented as paper C4.5 at the 1988 Intern. Cryog. Eng. Conf. Southampton, July 12 - 15, 1988 .

EXPERIMENTS

The zero net mass flow (ZNMF) mode of the two-fluid model is established. Heat flow takes place during counterflow of normal fluid and superfluid in the porous plug. One side of the plug is connected to a heating chamber, the other side to an external He II bath. A transient technique is employed, imposing a step input in power externally. The resulting thermograms T(t), e.g. Figures 1 and 3, are considered subsequently.

The porous media (inset of Figure 2) are sintered stainless steel plugs with axis oriented vertically. The chamber walls are made out of phenolic (Fig. 2, outer diameter 1.5 cm, overall length 3.6 cm). The heater is wound bifilarly to a resistance near 100 ohms using constantan wire (75 μm diameter). The plugs have the following dimensions: PKS: diameter D = 6.4 mm; thickness L = 0.75 mm; PSM 05: d = 7.9 mm; L = 1.75 mm; PSM triple: D = 3.23 mm; thickness of the single plug: L = 1.6 mm, resulting in a total thickness of 4.8 mm.

THERMOGRAMS AND POROUS PLUG PHASE TRANSITION RECORDS

The T(t) curves observed show single phase regimes, phase change onsets, and evolution of domains involving triple-phase modes of heat flow.

(a) Single-phase He II modes

Two principle regimes of transport are observed in the T(t) thermograms. At low step inputs in power, the temperature rises monotonically with $dT/dt > 0$, toward a final steady temperature difference with respect to the outer bath (Fig. 1). The normal fluid flows in the laminar regime with a superficial heat flux density, q per total plug cross section A, i.e. $\dot{Q} = qA$. The q value is related to a superficial normal fluid velocity (approach velocity) of

$$v_{no} = \kappa_n |\, \mathrm{grad} P_T \,| / \eta_n \tag{1}$$

(η_n shear viscosity of normal fluid, κ_n normal fluid Darcy permeability of the sintered plug). The driving pressure difference, established at very small velocities, is London's thermomechanical difference ΔP_T.

$$\Delta P_T = \rho S \Delta T\,; \quad \Delta T \ll T \tag{2}$$

(ρ liquid He II density). The single-phase He II mode is terminated at the critical value ΔT_c.

$$\Delta T_c = \mathrm{const}(\rho_s/\rho_n) L_c^3 \rho \,|\, \Delta P_T \,| / (L \eta_n^2) \tag{3}$$

The constant is found to have a particular value for each plug. The characteristic length is $L_c = (\kappa_n)^{1/2}$.

The non-linear regime is established above ΔT_c. There is a quantitatively different rate of temperature rise (dT/dt) initially. At long times, $q_o = \dot{Q}/A$ is considerably less than the wide duct value for the same ΔT.

(b) Phase transition phenomena at moderate heat input

The onset of a phase change is marked in the present thermograms by a change of the temperature-time derivative from positive to negative values, e.g. Fig. 1 (runs 2 and 3). In principle, such a change may be produced via the mechano-caloric effect. However, the ZNMF mode in the relatively wide pore sized range covered appears to lack such a behavior with $dT < 0$. The vaporization phenomenon causing the relative lowering of the liquid chamber temperature to $dT/dt < 0$ appears to utilize the existing excess enthalpy of heated He II in the chamber. This implies a superheating of He II across the vapor pressure curve phase diagram (Fig. 6). Related onset values are given in Table I.

Table I. Thermogram data $\dot{Q}_t(t_t)$ for onset of vapor formation
[plug Pk 10-S-02-6.6x0.75; Bath: T = 2.6 K]

$\dot{Q}_t$	Time t, sec
0.171	0.44
0.153	0.556
0.123	1.04
0.115	1.48

Above $\dot{Q}_t$, temperature oscillations are observed in a discrete $\dot{Q}$-range during the step power input. No final steady value is found. Instead, the non-linear oscillations persist around a mean T value. These patterns are reminiscent of previous observations, however there have been pattern variations from one plug to the next. The onset time t_t appears to change with $\dot{Q}$, similar to $\dot{Q}_t(t_t)$ in Table I.

(c) Phenomena at high heat input

At high q, oscillations may occur, as in (b). However, there is only a restricted duration of liquid T variations at temperatures not far from T_λ. Figure 3 is a high-q thermogram. After the initial pattern of type (b), the liquid temperature rises sharply to T above the thermodynamic critical temperature T_c = 5.2 K (Fig. 6).

Figure 4 is a plot of the thermal conductance $\dot{Q}/\Delta T$ derived from the thermogram (Fig. 3), assuming steady heat flow. For the plug area on the order of 0.1 cm^2, the ratio of $q_o/\Delta T$ attains the order of 10 $W/(cm^2\ K)$. This high value indicates that heat flow through the plug is not deteriorated seriously prior to the T-excursion. The rapid drop of $\dot{Q}/\Delta T$ in Fig. 4 signals film boiling conditions.

Figure 5 shows vaporization onset conditions, corresponding to (b), as $\dot{Q}$ versus ΔT. The ΔT values do reach into the metastable He II domain signaling *superheating* across the vapor pressure curve. The inset of Fig. 5 is a plot of ΔP, recorded by a differential P-transducer on plug (PA/FA PSM 01S-tr-3.2x1.6). The ΔP-records show an insignificant increase in pressure in the non-linear regime (a) of a few millibar.

The phase diagram P(T) contains the low-P extension of the lambda line and the homogeneous superheat limit.[1] A few data points of (b) at and near vaporization onset are included in Fig. 6. Further, several *high* ΔT values are marked. It is noted that there is no chance to find metastable liquid, for an extended period of time, in the region beyond the homogeneous nucleation limit.

CONCLUSIONS

From the present porous media thermograms it is concluded that our plugs display phase change phenomena consistent with phenomena observed in larger duct systems connected by the counterflow mechanism to a heated He II reservoir.

Acknowledgment. After initial seed support by the UCLA Senate Research Committee, the investigations have received partial support by NASA Ames Research Center. We acknowledge this along with the help and input of the Cryogenic Lab. group, in particular, Messrs. F. Afifi, Herbert Simanjuntak and David Ono.

REFERENCES

1. Nishigaki, K. and Saji, Y. Superheating in He II and Successive Phase Transitions in Metastable States. Phys. Rev. B 33 (1986) 1567.

2. Helvensteijn, B. P. M. and Van Sciver, S. W. Metastable Heat Flow Phenomena and Drooping Pressure Differences in He II Using Multiple Channel Configurations, Adv. Cryog. Eng. (1988) 33.

3. Fouaidy, M. and Francois, M. X. Heat Transport Properties of Pressurized and Saturated He II in the Vicinity of T, Adv. Cryog. Eng. (1988) 33.

4. Chuang, C. Ph.D. Thesis, University of California, Los Angeles, 1981; Chuang, C. et al., Transient Triple-Phase Transitions in Superfluid Liquid He II, Adv. Cryog. Eng. (1982) 17 493-500.

5. Caspi, S. and Frederking, T. H. K. Triple-Phase Phenomena During Quenches of Superconductors Cooled by Pressurized Superfluid Helium II, Cryogenics (1979) 19 513-516.

6. Rybarcyk, L. J. and Tough, J. T. Superconducting in He II and the Extension of the Lambda Line, J. Low Temp. Phys. (1981) 43 197.

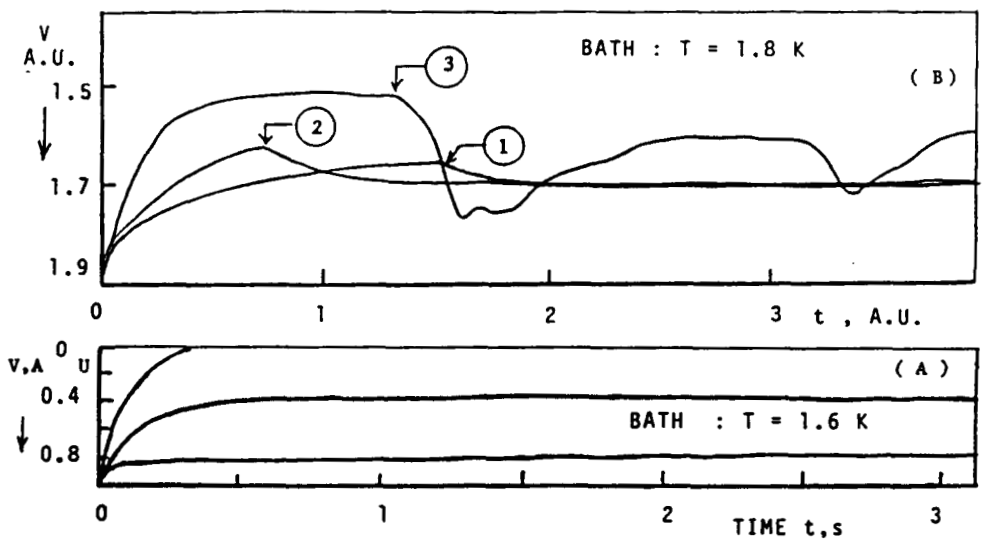

Fig.1. Thermograms for step power input to heater ;(heater current I); V thermometer voltage (in arbitrary units A.U.); Plug PK K 10 S 02-6.4 x 0.75 ;
A. Low power,imposed as step input in the single-phase He II regime ;
B. Intermediate power showing onset of vaporization and oscillations of the temperature in the chamber liquid ; Heater current I : ① 37 mA ; ② 45 mA ; ③ 55 mA .

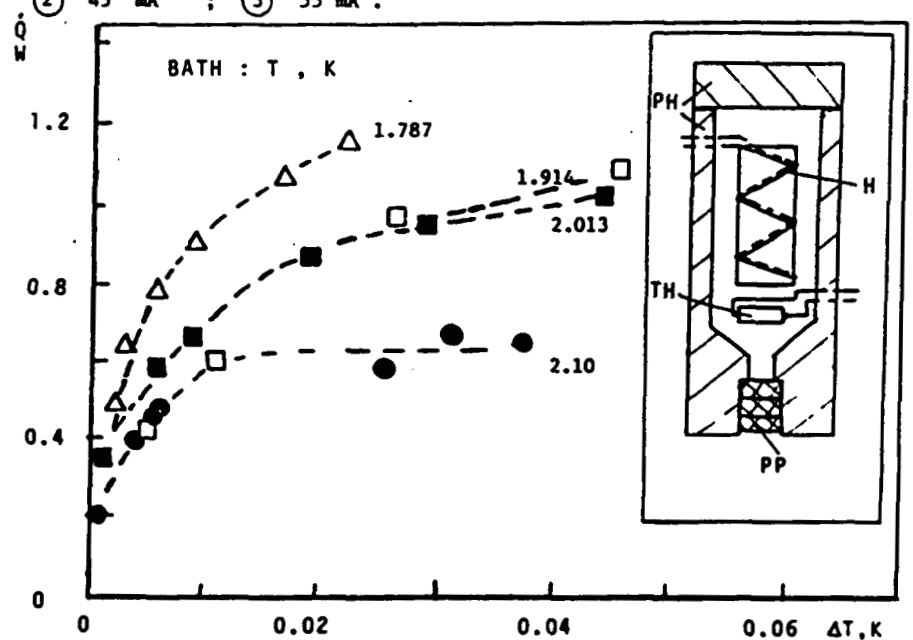

Fig.2. Heat flow rate $\dot{Q}$ versus ΔT for long times (t) [steady heat flow]; plug PA/FA PSM 01 S-tr3.2 x 1.6 ;
Inset : Schematic of porous plug system for zero net mass flow ; H heater ; PH phenolic sleeve ; PP sintered porous plug ; TH carbon resistance thermometer.

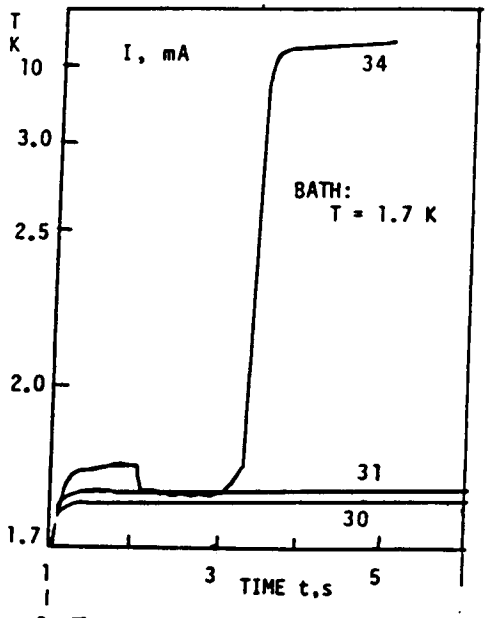

Fig. 3. Thermogram : Temperature T(t) for step input in power to heater carrying current I ;
Plug : PA/FA PSM 01S-tr- 3.2x1.6

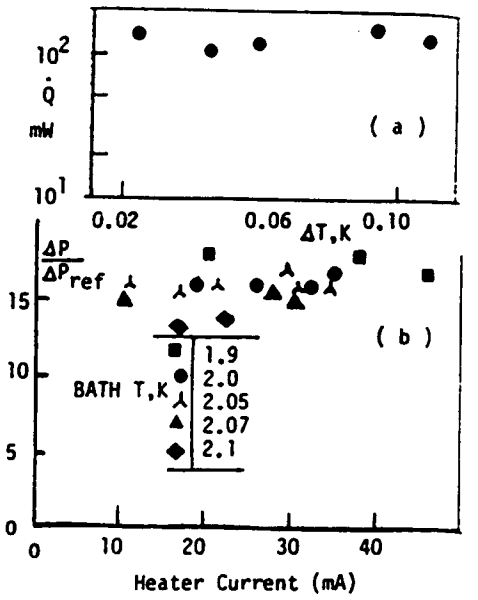

Fig. 5. a. Heat input for the onset of vaporization vs. ΔT
b. Normalized pressure for heater carrying current I

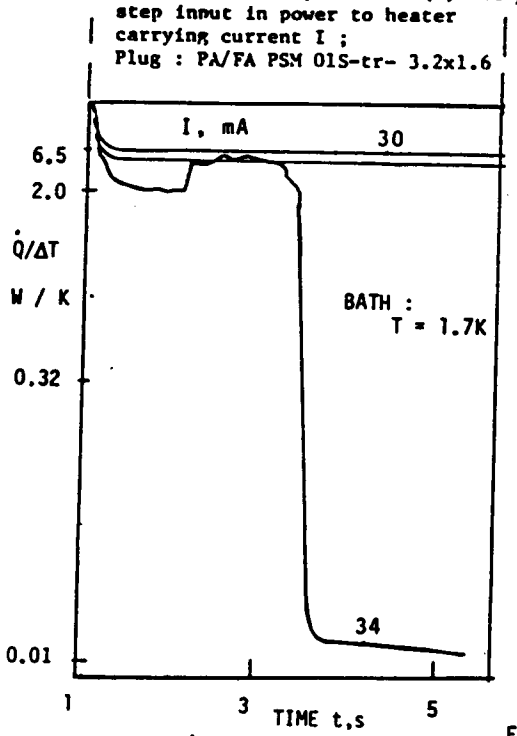

Fig.4. Ratio of Q̇/ΔT (thermal conductance) vs. time, of Figure 3 .

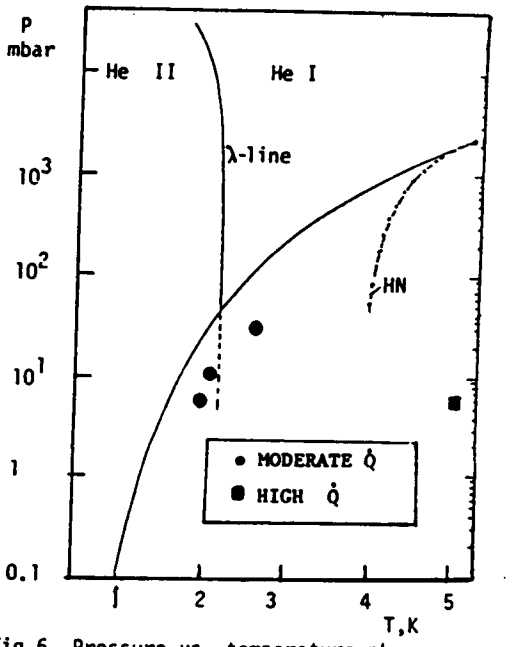

Fig.6. Pressure vs. temperature phase diagram (He^4); HN Homogeneous nucleation limit; Data: Thermogram type Fig. 3.

APPENDIX $\tilde{B}$ **

CRITICAL TRANSPORT PARAMETERS FOR POROUS MEDIA SUBJECTED TO COUNTERFLOW

T. H. K. Frederking, F. A. Afifi, D. Y. Ono
University of California, Los Angeles, CA 90024

Experimental and theoretical studies have been conducted to determine critical parameters at the onset of non-linear counterflow in He II below the lambda point of Helium-4. Critical temperature differences have been measured in porous media for zero net mass flow and for Darcy permeabilities in the order of magnitude range from 10^{-10} to 10^{-8} cm^2. The normalized critical temperature gradients, which covered the liquid temperature range of 1.5 K to the lambda temperature, are found to vary with T proportional to the ratio of the superfluid density to the normal fluid density. This liquid temperature dependence appears to be consistent with duct data which are limited at low temperature by a Reynolds number criterion.

**) Presented at the 1988 Space Cryogenics Workshop
Frascati , July 18-19, 1988.

Introduction

There have been numerous reports on "critical" transport parameters at various flow transitions of superfluid liquid He II below the lambda point. The two-fluid model, a most successful concept, has permitted considerable progress in the phenomenological description of the various transport phenomena in He II. According to the basic two-fluid postulate there is superfluid, the quantum liquid capable of motion without friction, and normal fluid carrying entropy $\dot{S}$ and heat $\dot{Q}$. Both transport rates ($\dot{S}$ and $\dot{Q}$) are subject to dissipation by friction processes.

One set of critical parameters is concerned with superfluid, in particular with its zero resistance flow limits at superfluid critical velocities. Another set of criteria addresses questions of flow transitions in heat and entropy convection. Because of viscous forces impeding normal fluid motion, there is a finite resistance in all regimes of normal fluid motion. Thus questions come up in many application areas concerning the prediction of critical rates. It is the purpose of this work to present results of critical temperature difference parameters for porous media subjected to counterflow (ZNMF). Despite the restriction to heat flow conditions, it is noted that mass effects associated with *superfluid* (e.g. superfluid density ρ_s) may enter critical parameters. Therefore, a brief discussion of several critical rates is presented first. Subsequently, the discussion will focus on the experiments. From the data sets collected, we obtain criteria inspected in their temperature behavior. Finally, the present experimental data are compared with other results and conclusions are presented.

Critical quantities and major transport modes

Critical Superfluid Flow. One set of criteria relates to the transition from resistance-less "superflow" to resistive flow. The "superflow" cessation has been formulated in terms of quantum constraints for He II. At the onset of resistance, quantum vortices are generated causing vortex shedding into the liquid. The kinematics of these Onsager-Feynman quantum vortices

has been modeled by Feynman[1] and others (compare study by Ladner[2]). For instance, at the exit of a tube the shedding of "smoke ring"-like vortices has been envisioned as the critical process. The resulting critical velocity is proportional to the quantum of circulation ($h/m = 10^{-3}$ cm^2/s), and it is inversely proportional to the tube radius (D/2). Very small critical superfluid velocities result for radii larger than 1 cm.

Another critical flow rate is predicted by the Piteavskii–Mamaladse[3] version of the Landau theory of higher order phase transitions[4]. Starting from basic superfluid parameters, it has been possible to quantify critical velocities of superfluid orifice flow[5]

Critical Counterflow. A different class of criteria pertains to counterflow of superfluid and normal fluid, involving a finite heat flow rate, at zero net mass flow (ZNMF). A special case has been the Dimotakis criterion[6] relying on the mutual friction parameter of the Gorter-Mellink transport concept for counterflow[2]. The present simplified view of this criterion ignores the various transition steps known for ducts with adiabatic walls (ZNMF ducts). Details of the transition have been studied and surveyed[7,2]. In the present porous media however, a *finite* pore size distribution masks the "fine structure" of the transition. Therefore, the present simplified approach ignores these details concentrating instead on steady values (usually obtained for externally imposed decreasing heat flux densities ($dq < 0$)). In this manner, hysteresis effects, leading to large critical rates at vortex shedding onset, are de-emphasized. The Dimotakis result for the critical counterflow velocity ($(w_c = |v_c - v_s|_c)$ is written as

$$w_c = (1/\pi)/[D\rho A_{GM,c}] \tag{1}$$

(D duct diameter, ρ liquid He II density). The mutual friction between vortex lines generated from superfluid and normal fluid excitations is described by the Gorter-Mellink function A_{GM}, a function of temperature T and pressure P. The critical value $A_{GM,c}$ has been documented only slightly. However for the asymptotic regime of chaotic counterflow, with size-independent q-values, rules of similitude have been introduced[8]. The Gorter-Mellink function of this similitude

approach for the high-q range is formulated in terms of basic thermophysical properties of He II

$$A_{GM} = K_{GM}(\rho/\rho_s)/\eta_n \tag{2}$$

(K_{GM} = const = 11.3, η_n shear viscosity of normal fluid). Starting from this high-q information, an order of magnitude estimate of the critical counterflow velocity (w_c) is considered: the high-q function for A_{GM} is substituted for the critical value at low $q = q_c$. One then arrives at

$$w_c = (K_{GM}^3/\pi)\eta_n(\rho_s/\rho)/[D\rho] \tag{3}$$

In the discussion of equation (3), it is noted that at low T we have a very small normal fluid density [$\rho_n \ll \rho$; ($\rho_s \approx \rho$)]. Furthermore, the critical counterflow speed approaches the critical normal fluid velocity ($w_c \approx v_{nc}$). Several authors have addressed this condition, noting that a normal fluid Reynolds number criterion ought to become valid as soon as the normal fluid speed increases significantly. According to the Reynolds number criterion, the total density has been used ($\rho = \rho_s+\rho_n$) with reference to normal fluid values in speed and shear viscosity

$$Re_c = v_{nc}\rho D/\eta_n \sim w_c\rho D/\eta_n$$

$$\rho_n \ll \rho \tag{4}$$

The corresponding counterflow criterion is then recast, paralleling the normal fluid Reynolds number. From equation (2) we obtain

$$Re_c \sim (K_{GM}^3/\pi)(\rho_s/\rho) \tag{5}$$

The constant (K_{GM}^3/π) turns out to be 459. In other words, this constant approaches the same order of magnitude as the classical Reynolds number for Newtonian fluid flow through ducts (Re_c = 2300). Thus, the simplest estimate, permitted by the present approach, appears to be a combination of statement (4) with the temperature dependence of equation (5). The resulting Reynolds number for normal fluid flow, using the total density, is written as

$$Re_c = Re_{ref}(\rho_s/\rho) \tag{6}$$

The heat flux density at zero net mass flow results from transport of (ρST) per unit volume at the speed v_n

$$q = \rho S T v_n \tag{7}$$

(S entropy per unit mass of liquid). Thus the normal fluid Reynolds number (4), at critical conditions, is equal to $q_c D/(\eta_n ST)$. Figure 1 presents data which provide only limited support for equation (6).

Critical temperature gradient condition. The dimensionless form of the critical T-gradient is formulated assuming a porous media geometry. The "classical" flow of Newtonian fluid at low speed has been described by Darcy's law. The mean speed of the fluid is conveniently expressed as approach velocity v_o (= superficial speed). Zero net mass flow studies at low temperature have led to the adoption of an analog of Darcy's law for the normal fluid. This particular equation has become quite useful for the characterization of several flow rate conditions[9]. The Darcy law analog is written in terms of the approach velocity for normal fluid flow (and heat flow).

$$v_{no} = \kappa_n |\, \text{grad}\, P_T \,| / \eta_n \tag{8}$$

The driving gradient is the thermomechanical pressure gradient, described by London's equation

$$\text{grad}\, P = \rho\, S\, \text{grad}\, T \tag{9}$$

The normal fluid permeability is κ_n. The Darcy permeability of a clean porous plug, without impurity condensate layers, ought to be very close (within 1%) to the room temperature value for Newtonian fluid, unless stress concentrations and other effects change geometric conditions. After insertion of equation (9) into (10) one may obtain a dimensionless form of Darcy's law analog, including the dimensionless T-gradient. Both sides of equation (8) are multiplied by $\rho L_c/\eta_n$. L_c is the characteristic length of the porous medium (with $L_c^2 = \kappa_n$). Because of the correspondence in terms of permeability, L_c is a measure of the fluid throughput capability of the

porous medium. The dimensionless result obtained is

$$\rho S \,|\, \text{grad } T \,|\, L_c^3 \rho / \eta_n^2 = v_c \rho L_c / \eta_n \tag{10}$$

The left hand side of equation (10) represents the dimensionless T-gradient, and the right hand side is again the normal fluid Reynolds number. At critical conditions the subscript c is introduced. One possible postulate for a quantification of critical counterflow is the condition of a superfluid density-dependent function. This implies a temperature-dependence with the constraint that Re_c approaches zero, as T approaches the lambda point (T_λ), while (ρ_s/ρ) decreases toward zero.

Another postulate, supported by literature data, is the adoption of a temperature-dependent (or order parameter-dependent) function of the dimensionless critical T-gradient, called $N_{\nabla T_c}$.

$$N_{\nabla T_c} = \rho \, S \,|\, \text{grad } T_c \,|\, \rho L_c^3 / \eta^2 \tag{11}$$

Investigations of porous media[10] and of a duct[11] suggest that $N_{\nabla T_c}$ varies from zero, at T_λ to finite values, proportional to (ρ_s/ρ), when T is lowered. Thus, there exists a critical number (N_c) such that the simplest counterflow criterion for a specified porous medium is

$$N_{\nabla T_c}(\rho_n/\rho_s) = N_c \tag{12}$$

The value of N_c is to be determined experimentally for a particular porous medium as long as further porous plug parameter effects are unknown.

Experiments

Experimental porous media studies have been conducted with sintered stainless steel plugs. The investigations have been quite similar to ZNMF studies of other porous media, e.g., reference 12. A chamber equipped with heater and thermometer is separated from a main He II bath by means of a porous plug (inset of Fig. 2). Other chamber walls are insulated. The wall material is phenolic (outer diameter of Fig. 2 [inset] is equal to 2.5 cm, overall length is 3.6 cm). The stainless steel plugs employed have the following dimensions: PKS plug, very thin disk with a diameter of D = 0.64 cm, thickness L = 0.075 cm; PSM plug, cut from a large disk, diameter D = 0.79 cm, L = 0.175 cm; PSM-type plug of small dimension, D = 0.323 cm, L = 0.16 cm. The latter plug has been arranged as a triple set, acting as three "flow resistances" in series. The sintered stainless steel plugs are mounted with axis oriented vertically. The heater inside the chamber has been wound using constantan wire (75 μm diameter) to approximately 100 ohms. The carbon resistance thermometers inside the chamber produce a thermogram, with non-linear T-scale recording the thermometer voltage versus time t.

The liquid He II inside the chamber can communicate with the outer liquid reservoir, permitting a very small mass inflow during initial heating. Heat removal by normal fluid, i.e. outflow out of the chamber, takes place during the ZNMF experiment. In contrast to previous studies,[12] a modification has been introduced. A transient technique is employed imposing an externally applied step power input to the heater inside the chamber.

Figure 2 is an example of the thermometer voltage versus time record at relatively low heater power. At moderate and high power inputs the thermograms obtained show additional features, such as onset of a phase transition, oscillatory modes of the temperature (T) versus time (t), and possibly large T-excursions into the vapor regime. The various phase transitions have helped in the diagnostics of the records, in particular identification of the critical rates. The final T-differences for steady transport, seen on the thermogram at long times, have been the basis for

the determination of critical parameters. At each bath temperature, the critical parameter set ($\Delta T_c[\dot{Q}_c]$) separates the linear transport regime (= laminar normal fluid flow) from the non-linear regime.

Small power inputs are necessary to cover the linear regime of (absolute) heat input $\dot{Q}$ versus temperature difference. Above the critical value, a non-linear $\dot{Q}(\Delta T)$-function is observed (e.g. Fig. 3). Figure 3 plots the approach heat flux density $\dot{Q}/A = q_o$ (A total plug cross sectional area). For most plugs, one obtains readily the permeability of normal fluid flow (κ_n) from the records, at least at low T. The defining equation (8), in conjunction with equation (9), may be expressed in terms of a property-dependent function $F(T) = [\rho S/\eta_n](\rho ST)$. We make use of the ZNMF equation for the approach heat flux density. From $q = \rho STv_{no}$, and $\dot{Q} = Aq_o$, one obtains

$$Q = A(\rho ST)\kappa_n \rho S[\Delta T/L]/\eta_n \tag{13}$$

After insertion of F(T), the normal fluid permeability is expressed as

$$\kappa_n = [\dot{Q}/\Delta T]LA/F(T) \tag{14}$$

At low T, the function F has very small values rising rapidly as T is raised. Therefore, for a specified heat input $\dot{Q}$, the ΔT-value in the linear range may be relatively large. In contrast, at "high" T, near the lambda point, only a small ΔT is established for the $\dot{Q}$-value specified. The inset of Figure 3 shows F(T).

Discussion of Results

Critical temperature difference function. Plug data obtained for long times as steady value $\Delta T(\dot{Q})$, provides a critical parameter set at the intersection of the linear characteristics with the non-linear function. Figure 4 presents the quantity $N_{\nabla T_c}/L_c^3$ as a function of liquid bath temperature. It is noted from equation (11) that the normalized critical T-difference involves the geometry only via the plug thickness (L). Further, there are only thermophysical He II properties aside from the ΔT_c-value. In Figure 4 all results obtained, within data scatter, and for the

temperature range covered, appear to be consistent with a variation of $[N_{\nabla T_c}/L_c^3]$ proportional to the superfluid to normal fluid ratio (ρ_s/ρ_n). It is noted that the density ratio has the value unity near 1.95 K. Therefore, an appropriate constant $[N_{\nabla T_c} L_c^{-3} \rho_n/\rho_s]$ may be read off directly from the log-log plot in Figure 4. The function $[10^{11}\ (\rho_s/\rho_n)]$ in cm^{-3}, has been included in Figure 4. Previous data[11] have been found to be proportional to (ρ_s/ρ_n) during early studies of a porous medium of high Darcy permeability.

Critical Reynolds number. The critical Reynolds number concept has been discussed primarily in early He II work using ducts.[2] In Figure 1 the critical Reynolds number equation (6) has been employed for a comparison. A reference critical Reynolds number of 2300 has been inserted. Various early data sets show little agreement with each other, presumably because of different techniques employed and because of different observation limits for critical conditions. However there are common tendencies. As T is lowered, starting from T_λ, there is a monotonic increase of the critical Reynolds number with $(T_\lambda - T)$. At low T, all of the data appear to indicate a tendency to increase less drastically in the (absolute) derivative $|dRe_c/dT|$. In fact, some data sets appear to level off at Reynolds numbers on the order of magnitude 10^3. Results by Chase[13] document this behavior.

Figure 5 is a plot of data[13] for four tubes with diameters which range from 0.08 cm to 0.4 cm. The inspection of Re_c provides support for the T-gradient criterion near the lambda transition. At low T however, the critical Reynolds number criterion appears to be a constraint. Thus, at this time we propose a simple empirical interpolation in the following form

$$Re = [Re_{ref}^{-4} + (\rho_n/\{\rho_s 550\})^{-4}]^{-1/4} \tag{15}$$

This function is included in Figure 5. It is seen that equation (15) describes the critical Re_c[13]-data quite well.

Conclusions

It is concluded that critical counterflow in porous media has a temperature dependence supportive of a dimensionless critical temperature gradient. This quantity is found to be proportional to the superfluid to normal fluid density ratio, for the data sets obtained in the present work, as far as the T-dependence is concerned.

Acknowledgments. The initial work has received UCLA Academic Senate seed funds (Grant 3526). The subsequent studies have been supported in part by NASA Ames Research Center. It is a pleasure to acknowledge the input of the Cryogenics Lab group, in particular of Messrs. P. Khandhar and P. Abbassi.

References

1. Feynman, R. P. Application of Quantum Mechanics to Liquid Helium. *Progress in Low Temp. Phys.* (Ed. C. J. Gorter), North-Holland, Amsterdam (1955) Vol. 1, 17.

2. Ladner, D. R., A Review of Superfluid Critical Velocities: Counterflow and Superflow in Channels of Simple Geometry. *Proc. Space Helium Dewar Conf.* (Ed. J. B. Hendricks and G. R. Karr), Univ. Alabama, Huntsville, AL (1984) p. 231.

3. Mamaladze, Yu. G., Parameters of Phenomenological Superfluidity Theory and the Lambda Point Shift. *Sov. Phys. JETP* (1967) 25 479-480.

4. Landau, L. D. and Lifshits, E. M. Statistical Physics, Pergamon (1958) Ch 14, 430.

5. Linnet, C., Amar, R. C., Wang, Y. G., Frederking, T. H. K. Superfluid Thermodynamic Transport Limits for Liquid Helium II. *Adv. Cryog. Eng* (1974) 19 365-373.

6. Dimotakis, P. E. Gorter-Mellink Scale, and Critical Velocities in Liquid-Helium Counterflow. *Phys. Rev. A* (1974) 10 1721-1723

7. Tough, F. T. Superfluid Turbulence. *Prog. Low Temp. Phys.* (Ed. D. F. Brewer) (1982) Vol. VIII, Ch 3.

8. Soloski, S. L., Frederking, T. H. K. Dimensional Analysis and Equation for Axial Heat Flow of Gorter-Mellink Convection (He II) *Int. J. Heat Mass Transfer* (1980) 23 437.

9. Yuan, S. W. K. Ph.D. thesis, Univ. California, Los Angeles (1985).

10. Frederking, T. H. K., Van Kempen, H., Weenen, M. A., Wyder, P. Critical Counterflow in Narrow He II-Filled Channels. *Physica* (1981) 108B 1129-1130.

11. Dorscheidt, A. G. F., Frederking, T. H. K., van Kempen, H., Wyder, P. Mutual Friction Evolution Near the He II-He I Lambda Transition, *Proc. 17th Int. Conf. Low Temp. Phys.*, (U. Eckern et al., Eds) North-Holland (1984) 305-306.

12. Lee, Jeffrey Marshall, M.Sc. Thesis, University of California, Los Angeles, 1983.

13. Chase, C. E. Critical Reynolds Number for Thermal Counterflow in Liquid Helium II. *Superfluid Helium* (Ed. J. F. Allen), Academic Press, London (1966) 215-229.

14. Griffiths, D. J., Osborne, D. J., Allen, J. F. The Nature of the Critical Velocities of Helium II Carrying a Heat Current. *Superfluid Helium*, Academic Press, London (1966) 25-37.

15. Vinen. Mutual Friction in a Heat Current in Liquid He II. IV. Critical Currents in Wide Channels. *Proc. Roy. Soc.* (1958) A243 400-413.

16. Brewer, D. F. and Edwards, D. O. Heat Conduction by Liquid Helium II in Capillary Tubes. II. Measurements of the Pressure Gradient. *Phil. Mag.* (1961) 6 1173-1181.

17. Chase, C. E., *Low Temperature Physics*, Butterworths, London (1962).

18. Vinen, W. F., *Proc. Roy. Soc.* (1957) A243 400.

19. Staas, F. A., Taconis, K. W., and van Alphen, W M., *Physica* (1961) 27 893.

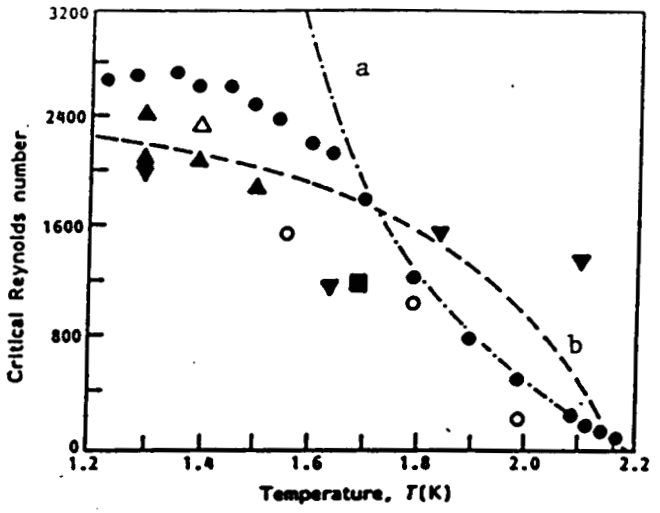

Figure 1 Critical Reynold's number *versus T*; (a), function $Re_c = 550\ (\rho_s/\rho_n)$; (b), Equation (6). ○, Brewer–Edwards, 108 m; ●, Chase, d = 0.159 cm; ▲, Griffiths *et al.*; ▲△, Vinen, 0.35 cm, 0.53 cm; ■, Staas *et al.*, 0.255 m

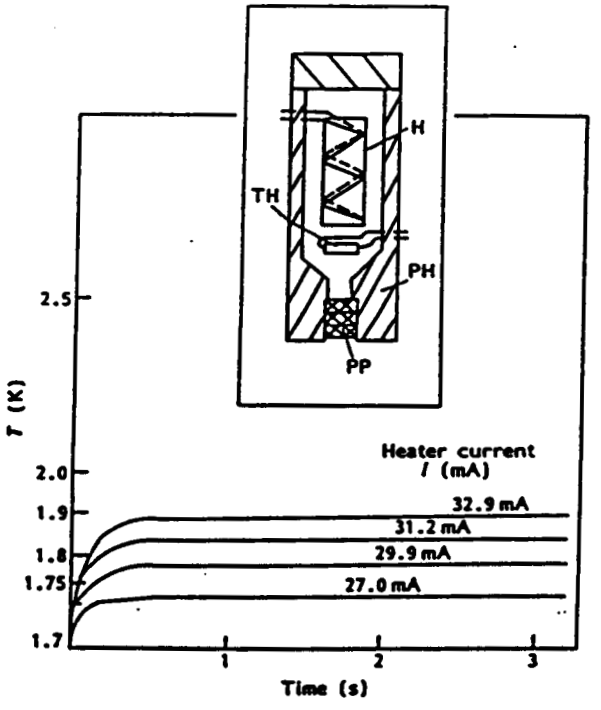

Figure 2 Thermogram: temperature *T versus* time; plug PA/FA PSM 01S-tr-3.2 x 1.6. Inset: schematic diagram of experimental apparatus with triple set of sintered stainless steel plugs. H, heater; PH, phenolic sleeve; PP, sintered Porous plug; TH, carbon thermometer

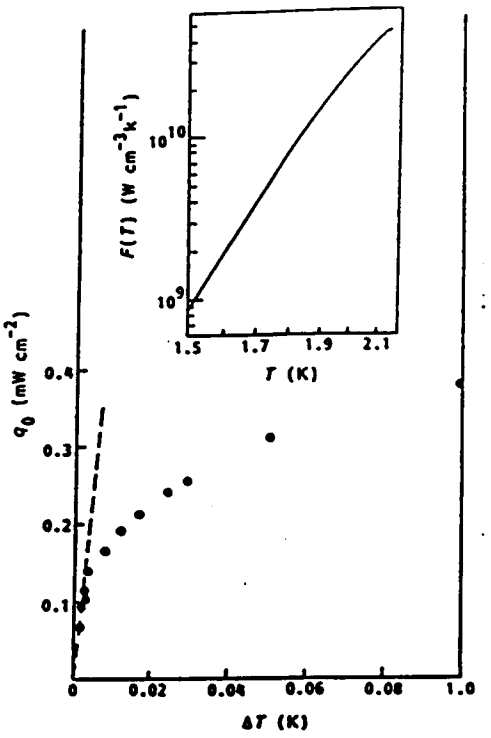

Figure 3 Approach heat flux density q_0 *versus* T at T_{BATH} = 1.91 K for plug K10S02-6.4 x 0.75. Permeability, $\kappa = 2.06 \times 10^{-10}$ cm^2. Inset: $F(T)$ of He II properties; Equation (14).

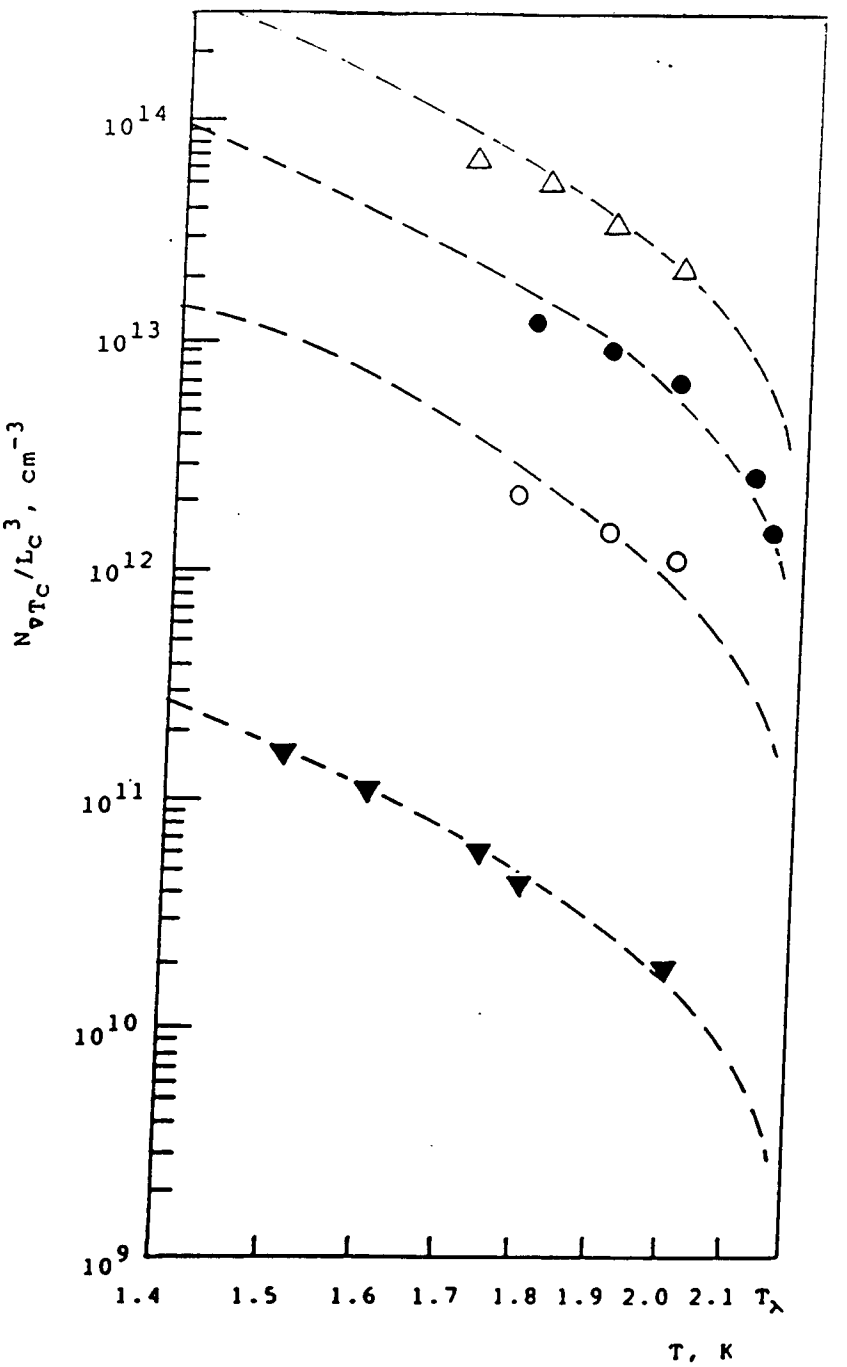

Fig. 4. Critical quantity $N_{\nabla T_c}/L_c^3$ as a function of temperature;
△ plug K 10 S 02-6.4x0.75 ; (2.2) (ρ_s/ρ_n) 10^{13} ;
• plug DO 01-S-05-7.9x1.75 ; 7.5 10^{12} (ρ_s/ρ_n) ;
o plug PA/FA PSM 01 S-tr-3.2 x 1.6 ; 1.3 10^{12} (ρ_s/ρ_n) ;
▼ porous medium , Ref. 10 ; 2.2 10^{10} (ρ_s/ρ_n) .

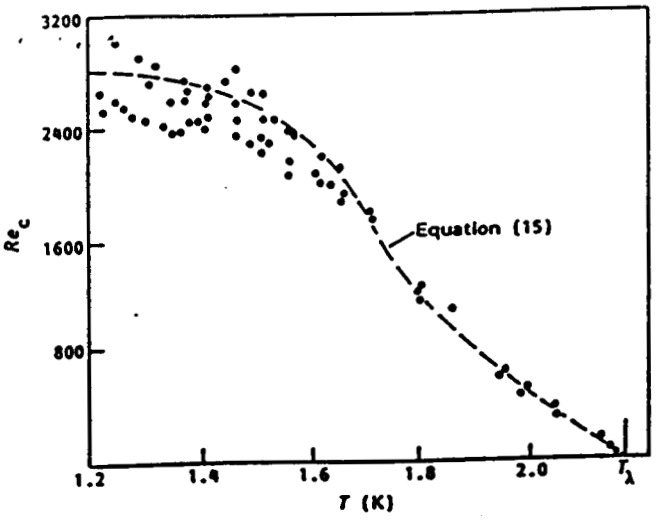

Figure 5 Critical Reynolds numbers of counterflow in ducts[13] (● full circles) *versus* temperature including interpolation of Equation (15)

APPENDIX C ++

CHARACTERISTIC PARAMETERS RELATED TO SUPERCONDUCTOR-COOLANT INTERACTION

T. H. K. Frederking

University of California, Los Angeles, California 90024-1592, USA

ABSTRACT

In the area of basic heat transfer mechanisms of Helium heat transfer and related influence on stability of superconducting magnets, thermal boundary conditions are among the sets of influential constraints. Important parameters, in particular characteristic lengths, are considered for the two sub-systems of a composite, i.e. solid state domains and fluid domains, noting examples of high transition temperatures.

++) Paper presented at the JOINT SEMINAR (US-Japan) on BASIC MECHANISMS OF HELIUM HEAT TRANSFER AND RELATED INFLUENCE ON STABILITY OF SUPERCONDUCTING MAGNETS, Aug. 29 - Sept. 2, 1988 , Fukuoka , Japan, paper of Session 1B

INTRODUCTION

The evolution of large superconducting magnets during the last 25 years has been based on the composite NbTi-Cu, a most popular metal superconductor (MSC). Its transition temperature T_c of about 9 K requires Helium-4 as coolant. The advent of high T (ceramic) superconductors (HTSC) in the last two years has posed questions concerning stabilization approaches (e.g.[1]) developed for Helium coolant systems. It is the purpose of the present investigation to inspect the conditions of superconductor-composite stability. The emphasis is on thermodynamic and transport phenomena related to the sizing of stabilizers. First solid state equilibrium is considered, subsequently fluid domains for both Newtonian and superfluid (non-Newtonian fluid) are inspected. Finally examples of interactions between composite and coolant, involving solid and fluid parameters, are presented.

CHARACTERISTIC SUPERCONDUCTOR PARAMETERS

The thermodynamics of a superconducting system is referred to using simplified assumptions associated with "superconducting electron fluids" and with "normal electron fluids". The extended Ginzburg-Landau (GL) (e.g.[2]) thermodynamic theory is the basis, along with Tuyn's law, for the critical magnetic field, written as flux line density

$$B_c = B_o(1-t^2) \tag{1}$$

B_o zero Kelvin value; $t = T/T_c$; T temperature. The related "two-fluid" number density is

$$n_s = n_o(1-t^4) \tag{2}$$

n_s = number density of electrons participating in the ordering process leading to low lying superconducting energy states.

There are three important lengths: 1) the electronic mean free path $(MFP)_e$; 2) the coherence distance (ξ); and 3) the (weak field) penetration depth (λ_p) for the exclusion of magnetic flux from bulk material (Meissner effect). There are two basic types of matter[3]: type I superconductors characterized by a ratio $\kappa = (\lambda_p/\xi)$ below unity, and type II superconductors with large κ values. Type I is characterized by the thermodynamic critical field (B_c of Eq. (1)). Type II material is characterized by two critical magnetic fields (B_{c1} and B_{c2}). At the lower critical magnetic field (B_{c1}), quantum flux lines start to penetrate into the superconducting bulk material. At the upper critical magnetic field (B_{c2}) flux line thread-

ing of the bulk material is complete such that the normal state is restored. MSC materials used for magnets have κ values on the order of magnitude of 100. The ξ values approach the order of the relevant lattice constant, i.e. values of atom spacing in the lattice. HTSC appear to show similar features with additional constraints of anisotropy. Nevertheless, it appears to be possible to arrive at estimates also for these systems assuming significance of the extended GL theory (Appendices A and B) for magneto-thermodynamic order of magnitude estimates. The parameter set comprises B_c and the number density (n_s) of the condensation process.

Figure 1 displays the critical current density at zero field expressed as ratio (j_c/B_o), for a transition temperature of 90 K. The thermodynamic result for $B_{c2} = \sqrt{2}\,\kappa B_c$ is (Appendices B and C)[4,5] (n_o = number density of T = 0 K)

$$j_o = [B_{c2}/(\sqrt{2}\,\kappa)][2/3]^{3/2}2e[n_o/(m_e\mu_o)]^{1/2} \tag{3}$$

With MSC materials, high j_c values have been realized with suitable thin films. For HTSC it appears to be reasonable to expect potentially useful results for similar films of high quality with flux pinning. The anisotropy of the HTSC materials however introduces different number densities (n_s) in different directions, causing anisotropic critical current densities j_c.

The simplified ideal thermodynamics leaves open considerable questions about stability of flux lines and stability with respect to dissipative events elsewhere (e.g. boundaries of coolant domains subject to phase transitions). There is field penetration into magnet material during magnet energization. During fast flux line motion, adiabatic conditions may prevail. Interdependence between critical current and line motion requires rate control by suitable pinning conditions. Because of normal states in vortex cores, and because of the necessity to bring in flux lines into the superconductor, dissipation is present. This causes magnetothermal heating influenced by temperature-dependent effects: the critical current density decreases with T while the heat capacity increases. There is the potential for adiabatic flux jumps[6] with final $T > T_c$. Two major steps in the magnet developments have been stabilization using normal metal, ("N" = Cu, Al) as "shunts", and subdivision of the superconductor into fine filaments[1]. A simple energy criterion for "magnetic pressure" thermalization leads to an upper bound for the filament diameter (d_F) (Appendix D)

$$d_F = \{\beta(1/j_c)\mu_o^{-1}[2\mu_o\rho\bar{c}_p\Delta T]^{1/2} \tag{4}$$

For HTSC[6], with large enthalpy, d_F becomes rather large for moderate current densities. Large enthalpy differences, $\bar{c}_p \Delta T = [H(T_c)-H(T_B)]$, appear to be available for hydrogen-cooled HTSC[7], if safety concerns are secondary (ρ density).

In addition to filament concerns, the MSC magnet R&D work has relied on well defined cooling systems. The related heat transfer has been considered early in conjunction with normal metal shunts introduced by Laverick and Stekly[1]. The question for optimal cross sections has stimulated modeling of the scenario of a local quench. Relying on a stability parameter (α), the Joule dissipation of steady operation ("cryostatics") has to be proportional to the heat removal capability of the system. Fourier diffusion ought to occur from T_c down to the vicinity of the bath temperature (T_B). Governing parameters are the heat transfer coefficient (h), the stabilizer cross section (A_c), the fluid-wetted circumference (C_c) and the electrical resistivity of the stabilizer (ρ_e). The limit of stable operation is reached for α on the order of unity. The required area is

$$A_c \geq \alpha^{-1}\rho_e I_c^2/[hC_c(T_c-T_B)] \tag{5}$$

(I_c = critical current). If h is large, excessive cross sections can be avoided. If the fluid undergoes unfavorable phase transitions, leading to a low h, rather large A_c, and along with it low overall electrical current densities are reached. This enlarges the volume of a magnet specified for a set of constraints.

FLUID DOMAINS: NEWTONIAN FLUIDS

The abundant literature on fluid convection permits numerous order of magnitude assessments for steady transport. The heat transfer coefficient (thermal conductance h) is proportional to the Nusselt number (Nu). The latter is proportional to the thermal conductivity (k) which in turn is proportional to the specific heat. Other parameters for a specified flow regime may exert secondary effects (possibly large in terms of pressure drops). As pointed out by Reynolds, pressure drop and heat removal rates are coupled, presenting challenges to coolant duct optimization.

Forced convection. The characterization lengths for short winding elements may be laminar entrance lengths, e.g. boundary layer thicknesses (δ,δ_T) whose ratio depends on the Prandtl number ($Pr = \eta c_p/k$), η shear viscosity. Hydrodynamic boundary layer thickness[8]

$$\delta = 5[\eta x/(v\rho)] \tag{6}$$

Thermal boundary layer thickness

$$\delta_T = \delta/\sqrt[3]{Pr} \tag{7}$$

(v velocity, x distance from entrance of rather wide coolant duct). In turbulent fluid, vortex shedding involves large bundles of quantum vortices whose discrete nature is of no concern in "eddy distributions". The steady state vortex distribution of well developed turbulence has been characterized in terms of layer models (e.g. wall domain with laminar flow features, buffer layer).

Natural convection modes. The natural ("free convection") mode may appear to be attractive at first glance in part because of the lack of a pump requirement. However, h on the order of 0.01 W/(cm^2 K) is rather poor causing great concern upon inspection of Eq. (5). Thus, the loss-of-flow scenario, starting from a forced flow system, is an unpleasant one. Nevertheless, the possibility of high h values near the thermodynamic critical point (P_c,T_{cT}) has prompted research of phase transitions without latent heat above and near P_c. Because of He I and He II, there are numerous phase transitions in Helium-4. For HTSC in nitrogen, the supercritical states of forced flow are quite a bit away from the transposed critical curve (TCC). Thus, numerous phase transition possibilities of He near T_c of the MSC appear to be of no serious concern for HTSC.

An exceptional case has been the centrifugal buoyancy-induced free convection, e.g. in a SC generator for electromechanical energy conversion. Coolant duct boundary layers have a thickness

$$\delta_T \sim [(L_g k\eta)/(\rho c_p |\,\mathrm{grad}\, P_g|)]^{1/4} \tag{8}$$

with an "effective pressure gradient"

$$|\,\mathrm{grad}\, P_g| = |a(\rho_\infty - \rho)| \tag{9}$$

L_g is the length of winding package exposed to acceleration (a), e.g. "g", or centrifugal buoyancy $r\Omega^2$ (r radius, Ω angular frequency). For power station size a.c. synchronous generator windings, the superconductor may be cooled conveniently using the available gradient with gravitational acceleration (g) replaced by $r\Omega^2$. The order of 1000 g may be reached causing thinning of the boundary layers, Eq. (8). Coefficients h comparable to nucleate boiling coefficients may

be reached.

Phase transitions. The most popular case has been nucleate boiling with h on the order of 1 W/(cm^2 K) in He I. In contrast, the high T excursion leading to film boiling, is characterized for liquefied gases in pool situations by h values on the order of 10^{-2} W/(cm^2 K). The drastic lowering of h, by a factor of 100, has caused sufficient stability concern. Therefore, a different scenario has been formulated for the nucleate pool boiling cryostatics. The parameter (α_1) assumes the dual role of a safety factor and a stability number. For the maximum heat removal rate at the "peak" heat flux density (q_p) one ought to reach the highest current density if α_1 reaches unity. The stabilizer cross section is

$$A_c \geq \alpha_1^{-1} I_c^2 \rho_e / (q_p C_c) \tag{10}$$

There is a more conservative approach using the "recovery" value q_{min} at the minimum heat flux density of the boiling curve. The simplification of the pool boiling curve suggests replacement of q_p in Eq. (8) by q_{min} (and possibly replacement of α_1 by another value α_2). A rather drastic enlargement of the area A_c results from this procedure. A middle-of-the-road approach appears to be offered by the "equal area criterion"[1], adopting a mean value of the boiling curve heat removal rate with respect to the transition temperature T_c.

FLUID DOMAINS: SUPERFLUID He II

Bulk He II has a low thermal resistance and excellent transient heat removal capability. Therefore, surface domains, such as insulating layers, and the Kapitza resistance are "seen" easier than in He I. London has pointed out the convective nature of He II heat transport while recent research emphasizes vortex system behavior[9,10]. Quantum vortex bundles produce "mutual friction" retarding the flow of "normal fluid" which, in two-fluid model language, carries the entropy and the thermal energy of He I. Superfluid produces the thermomechanical effect, a pressure increase useful for thermally induced "forced flow". There is the benefit of independence from gravity force orientation.

Sizes of vortex bundles ought to affect the flow in narrow cooling passages. Phase separator data for space systems, e.g.[11] and zero net mass flow modes in similar porous media have shown that passages below the order of magnitude 10^{-3} cm do not permit high transport rates, predicted for bulk liquid, and desired for large He II-cooled magnets. This size influence has been represented by a fluid "rate constant" (K^*_{VLPS}, K^*_{ZNMF}). The latter is the ratio of an effective

counterflow speed, $v_e = [q/(\rho_s ST)]$ divided by the speed predicted from mutual friction of bulk He II (S entropy per unit mass),

$$K^* = v_e/[S\,|\nabla T|\,(\eta_n/\rho_n)(\rho_s/\rho)]^{1/3} \tag{11}$$

Figure 2 presents rate constants versus the Darcy permeability κ of a porous medium.

There appears to be an extraordinary richness in phase transitions at the low temperatures of He II. This may produce peculiar loss-of-flow quench scenarios. There are very attractive features related to the possibility of consistently high h values, a large enthalpy difference with MSC, a "heat pipe" like transport rate in the liquid for not too narrow cooling passages. In addition, the thermomechanical effect may be used for pumping of liquid through magnet windings without excessive mechanical (electrical) power taken from an external device.

SUPERCONDUCTOR-COOLANT INTERACTION

As illustrated by various stability parameters, there appear to be numerous possible approaches referring to the thermal boundary conditions in the form of h. Often, simplified boiling curves for pool geometries have been adopted in order to assess the "degree of stability". Experimentally, exceeding the limits ought to lead to a quench with a finite propagation velocity. In this regard not only the criticism of unrealistic heat removal functions but also the danger of arbitrary stabilizer area (A) enlargement appears to be worth noting. Minimum propagation zones (MPZ) (e.g. Ref. 12 of this seminar), may function as onset of quench spreading. However, for film boiling phase transitions, a stationary "hot gas" domain is possible while dissipated energy is conducted away by Fourier diffusion. This detrimental case is characterized by a thermal decay length of $L_D = [kA/(hC_c)]^{1/2} \sim (Dk/h)^{1/2}$ of relative large extent (D diameter of composite conductor). A possible situation of the MPZ is a minor T increase within the quenched region, a relatively short current sharing domain and a major decay over the length L_D on both sides of the quenched domain.

Unsteady energy deposition criteria permitted by the coolant appear to bring less conservatism and more attractive overall current densities to a magnet geometry. In conjunction with a.c. conditions, the lack of a universal coverage of superconducting equipment stability has been noted (Ref. 13).

In the present context a simplified example is considered using "nucleate cooling stability[14,15] for HTSC cooled by He I, liquid hydrogen and liquid nitrogen in nucleate boiling modes. The peak value q_p is the characteristic parameter for the coolant limit. The electrical resistivity (ρ_e) of Matthiessen's rule for Cu is the dissipative term's characteristic property. A residual resistivity ratio of 50 is assumed in conjunction with a simplified concentric cylinder conductor geometry (r = D/2; $2r_c$ = superconductor diameter). The overall current density limit is obtained from $\alpha_1 = 1$ as

$$\bar{j} = [(2q_p/\rho_e)(r^2 - r_c^2)/r^3]^{1/2} \tag{12}$$

Optimization of j with respect to r, for a constant r_c, results in a maximum of $j = \bar{j}^*$

$$\bar{j}^* = [4q_p/(3\rho_e r)]^{1/2} \tag{13}$$

Figure 3 is a plot of $\bar{j}^*$ versus T using peak heat flux densities of nucleate boiling curves with emphasis on Kutateladse-Zuber functions[16]. It is seen that there is a lack of a drastic order of magnitude change as one switches from one coolant to another one potentially useful for HTSC. The $\bar{j}^*$ values are on the order of magnitude 10^4 A/cm^2 near maxima of the $\bar{j}^*(T)$ functions. This is in contrast to the potentially large intrinsic critical current densities, in zero field, of the thermodynamic model equation (3). In the presence of premature flux jumps, models for these phenomena[17] may be useful.

Acknowledgments. The recent porous media work has received partial NASA support. The efforts of the Cryogenics Lab collaborators are acknowledged with thanks. Romeo Carandang has calculated Fig. 1, Herbert Simanjuntak tried to extract meaningful q_p functions from the boiling system literature[16], P. Khandhar contributed porous media information. Mrs. Phyllis Gilbert's efficient processing of this paper and preceding manuscripts is very much appreciated.

REFERENCES

1. Wilson, M. N., Superconducting Magnets, Clarendon, Oxford, 1983.

2. Van Duzer, T., and Turner, C. W., Principles of Superconductive Devices and Circuits, Elsevier, New York, 1981.

3. Olsen, J. L., and Egolf, Swiss Chem. **9** 45 1987.

4. Chang, Y. W., et al., Rept. UCLA ENG-7109, 1971.

5. de Gennes, P. G., Superconductivity of Metals and Alloys, Benjamin, New York, 1966.

6. Wipf, S. L., Intern. Cryog. Eng. Conf. ICEC 12, Southampton, July 1988.

7. Green, M. A., Intern. Cryog. Eng. Conf. ICEC 12, Southampton, July 1988.

8. Schlichting, H., Boundary Layer Theory, 4th Ed., McGraw-Hill, New York, 1960.

9. Wilks, J. and Betts, D. S., An Introduction to Liquid Helium, 2nd Ed., Oxford, 1987.

10. Van Sciver, S., Helium Cryogenics, Plenum Press, 1986.

11. Yuan, S., Ph.D. Thesis, Univ. of California, Los Angeles, 1985.

12. Eckels, P. W., paper presented at this seminar.

13. Altov, V. A., Lvovsky, Yu. M., and Sytchev, V. V., Cryogenics **27** 121 1987.

14. Whetstone, C. N., and Boom, R. W., Adv. Cryog. Eng. **13** 68 1968.

15. Carruthers, K., Cornish, D. N., and Hancock, R., Proc. ICEC 1, Heywood-Templeton, London, 1978, p. 107.

16. Frost, W., Heat Transfer at Low Temperatures, Plenum, New York, 1975.

17. Akachi, T., Ogasawara, T., Yasukochi, K., Jap. J. Appl. Phys. **20** 1559 1981.

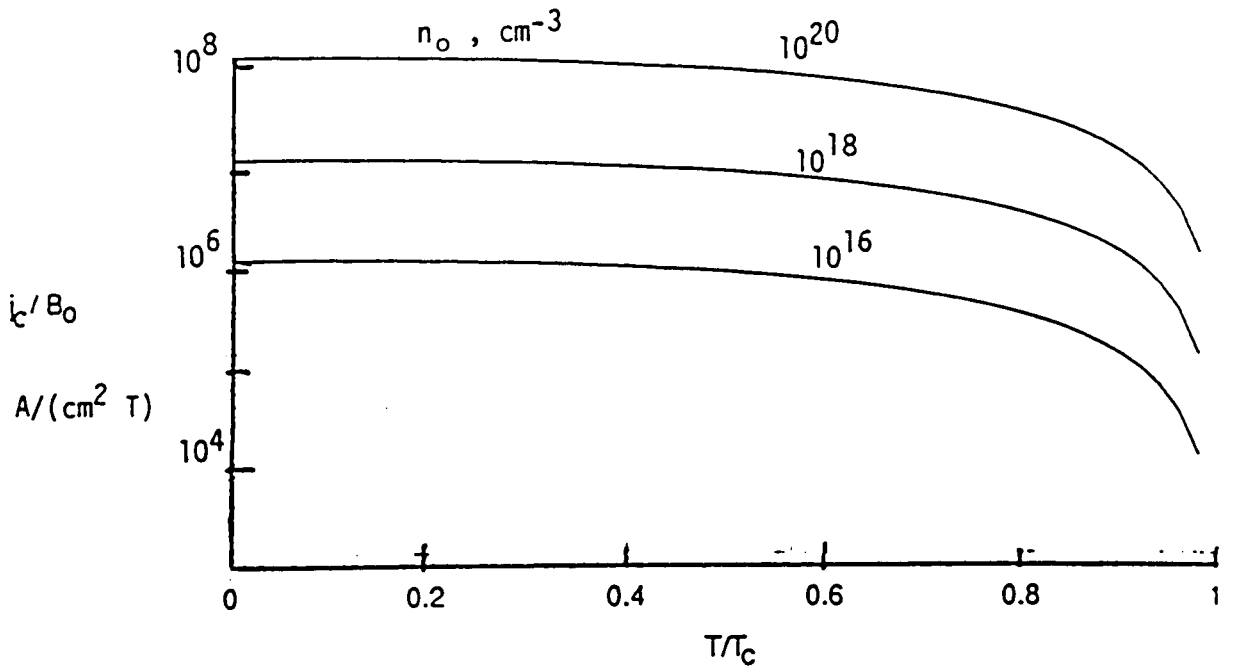

Fig. 1. Intrinsic critical current density expressed as ratio j_c/B_o versus temperature ratio

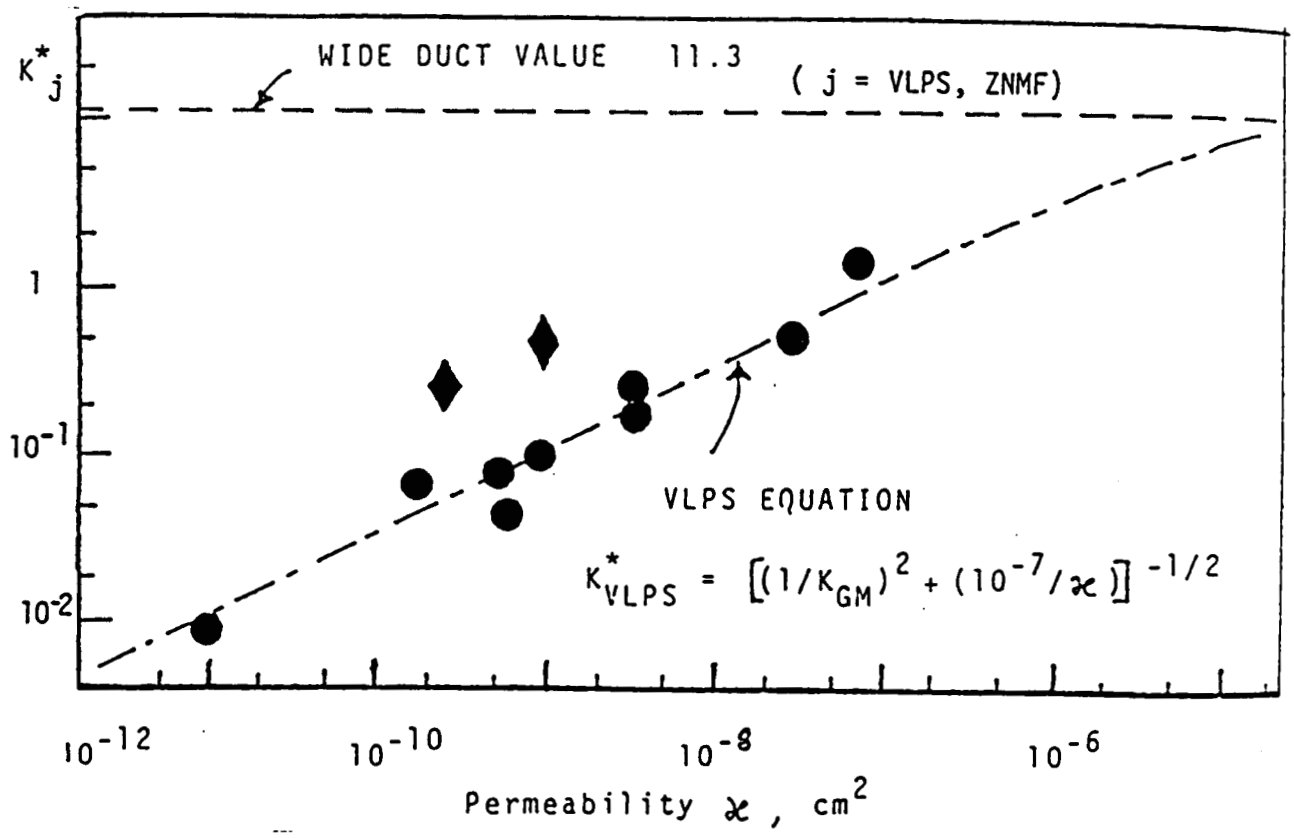

Fig. 2. Mutual friction "transport rate constants" K_j^* (j = VLPS, ZNMF) as a function of the Darcy permeability for porous media;

◆ zero net mass flow mode

● VLPS vapor liquid phase separation mode.

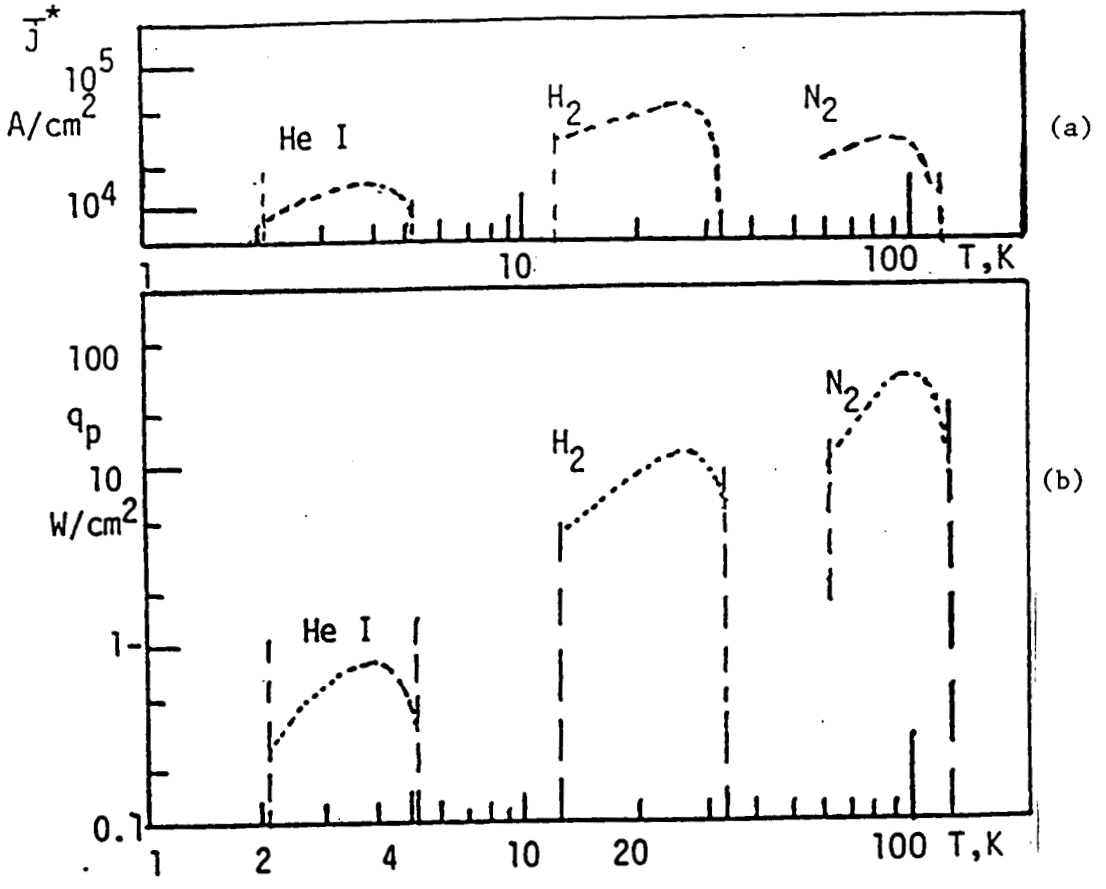

Fig. 3. Transport parameters of nucleate boiling and superconductor/boiling liquid interaction:

a. Peak heat flux density of nucleate boiling of saturated liquid;

b. Optimum overall critical current density of composite; radius D/2 = 0.2 cm; RRR = residual resistivity ratio 50; Cu.

APPENDIX A. MAGNETIC FIELD PENETRATION DEPTH (WEAK FIELD CONDITIONS)

Consider a boundary between "vacuum" and a type I superconducting state. The applied magnetic field is parallel to the surface of the superconductor. The shielding currents associated with the Meissner effect decay in a domain of finite thickness, and so does the field inside the superconductor. The energetics of this situation is considered minimizing, in a simple model, the total energy, with respect to the distance L from the surface at z=0. One contribution is the magnetic pressure-related energy, per unit area, of $\Delta P_m L = LB^2/(2\mu_o)$. The other important contribution is the electron kinetic energy of $m_e n_s v^2/2$; n_s number density; m_e electron mass, v velocity; where $j_e = n_s e v$ is the electrical current density. The latter is related to B, applied at z=0. From curl $B = \mu_o j_e$ we obtain the dominant contribution: $j_e^2 \simeq [B^2/(\mu_o)]/L$. Minimizing the sum of the two contributions, $\partial E_{tot}/\partial L \rightarrow 0$, one obtains the magnetic field penetration depth

$$\lambda_p = [m_e/(n_s e^2 \mu_o)]^{1/2} \tag{A.1}$$

It is seen that the present energetic assessment contains only one parameter, e.g. n_s of Eq. (2) which influences the penetration depth.

APPENDIX B: SIMPLIFIED MAGNETO-THERMODYNAMIC SUPERCONDUCTOR MODEL

Consider a macroscopic superconducting system. The Ginsburg-Landau (GL) phase transition equations (e.g. Ref. 2,4) are used and extended to low temperatures. Phenomenological equations for the macro-wave function, with number density $|\psi|^2 \sim n_s$, have equilibrium state minima with respect to normal states. The free energy density is $g = g_n - \alpha|\psi|^2 + (\beta/2)|\psi|^4$. The equilibrium state free energy difference, between normal and superconducting states, is obtained as

$$\Delta g = n_s f(t) \alpha_o \tag{B.1}$$

Using similarity functions, e.g. Tuyn's law for the critical magnetic flux density, one arrives at simple functions of t ($t = T/T_c$). At T = 0 K, the GL functional has values

$$\alpha_o = 2\Delta P_o / n_o \tag{B.2}$$

and

$$\beta_o = \alpha_o / n_o \tag{B.3}$$

($\Delta P_o = B_o^2/(2\mu_o)$ = magnetic pressure difference, equal to the maximum free energy density difference). The number density $n_o = |\psi_{oo}|^2$ is quite low for commercial metal superconductors as only the fraction (T_c/T_F) participates in the ordering process ("condensation" of the Bose-Einstein kind in momentum space) [T_F Fermi temperature]. The temperature effects on the functions (α/α_o) and (β/β_o) are shown in Fig. B.1. Figure B.2 illustrates the lowering of the free energy density, expressed as $\Delta g/\Delta g_o$ versus $[|\psi|^2]^{1/2}$.

Concerning characteristic lengths, the following functions are obtained: the penetration depth (Appendix A) varies as

$$\lambda_p/\lambda_o = [1-(t^4)]^{-1/2} \tag{B.4}$$

Noting the GL definition of the coherence length $\xi = \hbar/[2m_e\alpha]^{1/2}$, we have

$$\xi/\xi_o = [(1+t^2)/(1-t^2)]^{1/2} \tag{B.5}$$

The term (α/m_e) may be expressed as kinetic energy. Considering $\oint v \cdot dl = N \cdot \Gamma_o$ around a quantum flux line (vortex line), we make use of the quantum of circulation $\Gamma_o = (2\pi\hbar/m)$ ($\hbar$ Planck's constant divided by 2π). The energetically favored

lowest quantum state, with number N=1 is inserted in the energy per mass:

$$(\alpha/m_e) = \mathcal{F}_o^2/(2\xi^2) = v^2/2 \tag{B.6}$$

($\mathcal{F}_o = \Gamma_o/2\pi$) flux quantum $\phi_o = 2\pi\hbar/(2e) = 2.07\text{x}10^{-15}$ Wb $= 2.07\text{x}10^{-7}$ G cm^2.

Physical constants

$e = 1.602\ 10^{-19}$ As

$m_e = 9.1095\ 10^{-31}$ Kg

$\mu_B = 4\pi\ 10^{-7}$ Ωs/m

$\hbar = 1.054\ 10^{-34}$ J–s

Reference value: $n_o = 1\ m^{-3}$:

$(j_o/B_o) = 0.1630\ (A/m^2)/T$ for T = 0 K

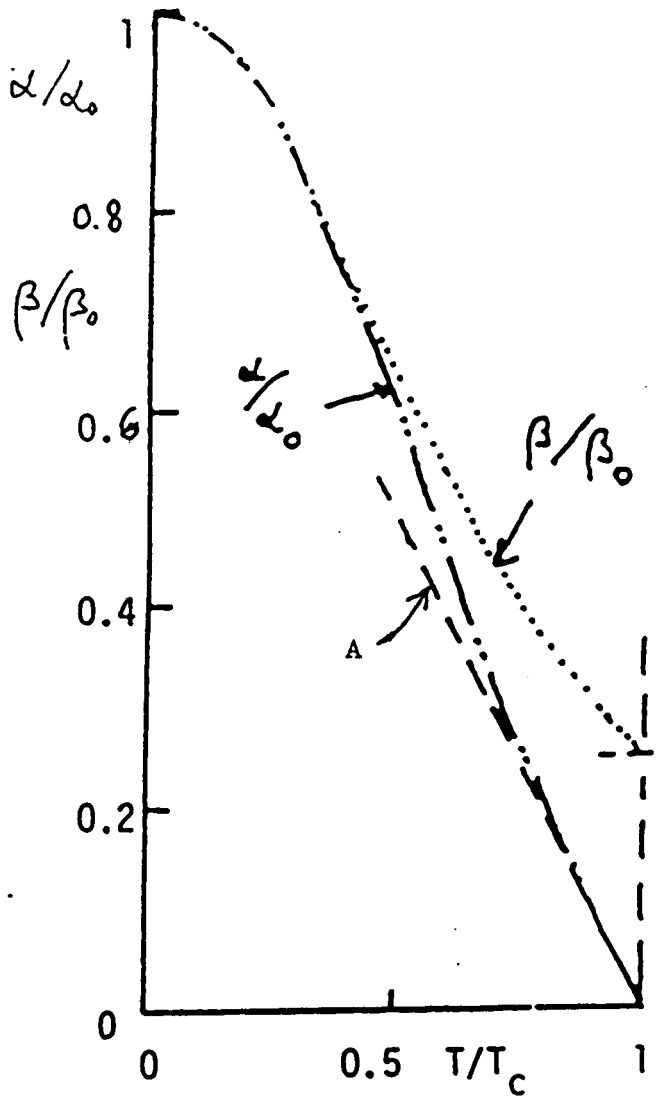

Fig. B.1. Ginsburg-Landau functions: α/α_o and β/β_o versus T/T_c; A = asymptote of energy parameter function α/α_o.

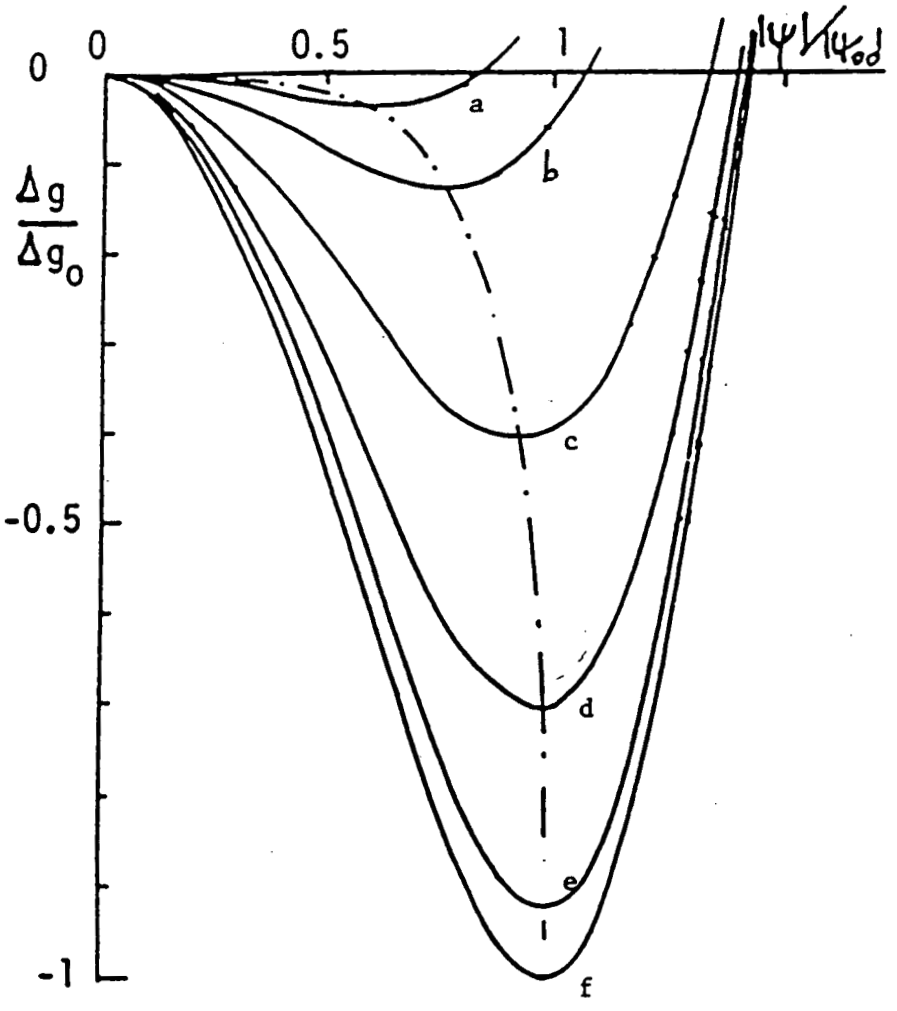

Fig. B.2. Free energy density difference ratio versus order parameter ratio; temperature ratios T/T_c: a = 0.9; b = 0.8; c = 0.6; d = 0.4; e = 0.2; f = 0 K.

APPENDIX C: SOLUTION FOR "UNIFORM FLOW"

The "intrinsic" solution for uniform flow (Eq. 3) derives from inclusion of the kinetic energy $(m_e/2)v^2$ in the free energy functional (v velocity of the "superflow" of electrons).

$$g = g - \alpha |\psi|^2 + (\beta/2)|\psi|^4 + (m_e/2)v^2 \tag{C.1}$$

The free energy is minimized with respect to $|\psi|^2$ for a constant temperature system at uniform flow. Further $j_e \sim (2e)|\psi_o|^2 v$ has a maximum value of j_c. Aside from the number density and constants, only thermodynamic quantities appear. Thus, an "intrinsic" value is reached. The difference Δg versus v has a point of inflection, leading to a situation similar to "choked nozzle flow". The limiting rate, Eq. (3), may be written in terms of Γ_o as

$$j_c = (4/3)3^{-1/2} e |\psi_o|^2 \Gamma_o / \xi \tag{C.2}$$

The energy per mass (α/m_e), Eq. (B.2) of Appendix B, relates to the thermodynamic magnetic pressure difference, i.e. to B_c. For T=0 one obtains

$$(\alpha/m_e) = \Gamma_o^2/(2\xi_o^2) = 2\Delta P_o/(\psi_\infty)^2 m_e = (B_o^2/\mu_o)/((\psi_\infty)^2 m_e) \tag{C.3}$$

Eliminating Γ_o from Eqs. (C.2) and (C.3) one arrives at

$$j_o = B_o \left[\frac{2}{3}\right]^{3/2} 2e \left[\frac{n_o}{m_e \mu_o}\right]^{1/2} 2^{1/2} \tag{C.4}$$

The temperature dependence of the critical current density is obtained readily (Appendix B).

$$j_c/j_o = (1-t^2)[1-t^4]^{1/2} \tag{C.5}$$

APPENDIX D: FILAMENT SIZE GUIDE LINES BASED ON SUPERCONDUCTOR ENERGETICS

Consider a thin slab ({filament model") of superconductor of width d_F with sufficient pinning centers. An externally applied field B produces an energy (per unit volume) proportional to the magnetic pressure difference

$$\Delta P_m = B^2/(2\mu_o) \tag{D.1}$$

Once a limiting condition with dissipation on the order of $j^2\rho_e$ (per unit volume) is attained, the enthalpy difference ΔH has to be sufficiently large to prevent "take-off" to high normal state temperatures:

$$j^2\rho_e \sim \rho[H(T_c)-H(T_o)] \tag{D.2}$$

where T_c is the transition temperature and T_o the superconductor temperature, assumed to be close to the coolant temperature. The enthalpy per volume $\rho\Delta H$ may be expressed in terms of the specific heat (per unit volume, of ρc_p), and in terms of the temperature difference $T_c-T_o = \Delta T$.

According to Maxwell's equation, curl $\vec{B} = \mu_o\vec{j}$, there is a current density on the order of

$$j \sim (B_e/d_F)\mu_o^{-1} \tag{D.3}$$

(D.3) is related to pinning models (e.g. Bean model) when $j = j_c$ is the critical current density of the limiting pinning strength. Equating the energy densities (D.1) and (D.2) one arrives at a field value (order of magnitude)

$$B \sim [(2\mu_o)\rho\bar{c}_p\Delta T]^{1/2} \tag{D.4}$$

Making use of (D.3), for the critical value, and of (D.4) we obtain a simplified limit for the filament of

$$d_F = \beta(1/j_c)\mu_o^{-1}[2\mu_o\rho\bar{c}_p\Delta T]^{1/2} \tag{D.5}$$

The factor β is on the order of magnitude unity. A metal superconductor is characterized by the following orders of magnitude:

Specific heat per unit volume: $\rho c_p \sim 10^3$ J/m^3 K)

Temperature: $\Delta T \sim 1$ K

External field value: $B \sim 1$ T

Critical current density: $j_c \sim 10^9$ A/m^2

The resulting filament size turns out to have the order of magnitude 10 μm.

APPENDIX $\tilde{D}$

ABSTRACT OF THE THESIS

The Characterization of Sintered Stainless Steel Porous Plugs for the Zero Net Mass Flow Mode of Helium II Including Nonlinear Flow

by

Parimal K. Khandhar
Master of Science in Chemical Engineering
University of California, Los Angeles, 1989
Professor Traugott H. K. Frederking, Chair

The Zero Net Mass Flow (ZNMF) transport mode of He II has been investigated. In this mode the normal fluid flow emitted from a heater is compensated by an inflow of the superfluid into the heating chamber using two-fluid concepts. Three sintered stainless steel plugs employed have Darcy permeabilities on the order of 10^{-10} cm^2; (10^{10} æ: 4.44 $\pm$ 0.03 #1, 2.06 $\pm$ 0.15 #2, 9.22 $\pm$ 1.0 #3). Because of limited data in the nonlinear ZNMF regime, heat flux densities (q) have been obtained as a function of temperature difference (ΔT) in this regime. The heat flux density is found to be permeability-dependent, $f(æ) = K_{ZNMF} = [(1/K_{GM})^2 + (æ_{crit}/æ)]^{-1/2}$, similar to the vapor liquid phase separation results of Yuan. The following semi-

empirical equation is proposed to fit nonlinear results.

$$q = [(1/K_{GM})^2 + (æ_{reff}/æ)]^{-1/2} \; [\rho_s^4 S^4 T^3 \eta_n |\nabla T|/\rho\, \rho_n]^{1/3}$$

$$æ_{reff} = 3 \times 10^{-10} \text{ cm}^2 \quad ; \quad \Delta T << T$$

(S entropy, ρ density, ρ_j (j = n, s : subscript n = normal fluid, s = superfluid), η_n = shear viscosity, K_{GM} = Gorter Mellink mutual friction constant = 11.3 for wide ducts. Two plugs tested are found to have $K_{GMF} = 0.3 \pm 0.01$ (#2) and 0.556 ± 0.04 (#3). An alternate equation has been deduced removing a conceptual difficulty of the above semi-empirical equation.

$$q = K_4/(L\, L_c)^{1/4} \quad [\rho_s^5 \; S^5 \; T^4 \; \eta_n^2 \; |\nabla T|/\rho^2 \; \rho_n]^{1/4}$$

(L = thickness of a plug, K_4 = Heat transport rate constant; 3.1 ± 0.2 (plug #2).

The present work has been extended up to the vaporization limit. The data exhibit superheating of He II across the vapor pressure curve.